Published online 23 March 2022

Nucleic Acids Research, 2022, Vol. 50, No. 7 ***3777–3798***
https://doi.org/10.1093/nar/gkac180

Xenogeneic nucleoid-associated EnrR thwarts H-NS silencing of bacterial virulence with unique DNA binding

Ruiqing Ma[1,6,†], Yabo Liu[1,†], Jianhua Gan[5,†], Haoxian Qiao[1], Jiabao Ma[1], Yi Zhang[1], Yifan Bu[1], Shuai Shao[1,4], Yuanxing Zhang[1,3,4] and Qiyao Wang[1,2,4,*]

[1]State Key Laboratory of Bioreactor Engineering, East China University of Science and Technology, Shanghai 200237, China , [2]Laboratory for Marine Fisheries Science and Food Production Processes, Qingdao National Laboratory for Marine Science and Technology, Qingdao 266071, China, [3]Southern Marine Science and Engineering Guangdong Laboratory (Zhuhai), Zhuhai 519000, China, [4]Shanghai Engineering Research Center of Maricultured Animal Vaccines, Shanghai 200237, China, [5]Shanghai Public Health Clinical Center, State Key Laboratory of Genetic Engineering, Collaborative Innovation Center of Genetics and Development, Department of Biochemistry and Biophysics, School of Life Sciences, Fudan University, Shanghai 200438, China and [6]Shanghai Public Health Clinical Center, Key Laboratory of Medical Molecular Virology of MOE/MOH, Fudan University, Shanghai 201508, China

Received November 09, 2021; Revised February 25, 2022; Editorial Decision March 03, 2022; Accepted March 07, 2022

ABSTRACT

Type III and type VI secretion systems (T3/T6SS) are encoded in horizontally acquired genomic islands (GIs) that play crucial roles in evolution and virulence in bacterial pathogens. T3/T6SS expression is subjected to tight control by the host xenogeneic silencer H-NS, but how this mechanism is counteracted remains to be illuminated. Here, we report that xenogeneic nucleoid-associated protein EnrR encoded in a GI is essential for virulence in pathogenic bacteria *Edwardsiella* and *Salmonella*. We showed that EnrR plays critical roles in T3/T6SS expression in these bacteria. Various biochemical and genetic analyses demonstrated that EnrR binds and derepresses the promoter of *esrB*, the critical regulator of T3/T6SS, to promote their expression by competing with H-NS. Additionally, EnrR targets AT-rich regions, globally modulates the expression of ∼363 genes and is involved in various cellular processes. Crystal structures of EnrR in complex with a specific AT-rich palindromic DNA revealed a new DNA-binding mode that involves conserved HTH-mediated interactions with the major groove and contacts of its N-terminal extension to the minor groove in the symmetry-related duplex. Collectively, these data demonstrate that EnrR is a virulence activator that can antagonize H-NS, highlighting a unique mechanism by which bacterial xenogeneic regulators recognize and regulate foreign DNA.

INTRODUCTION

Horizontal gene transfer of mobile gene elements (MGEs) is a major driving force shaping genome evolution in bacteria (1). Regarding Gram-negative bacterial pathogens, type III and VI secretion systems (T3/T6SS) and other various virulence determinants are encoded in horizontally acquired genomic islands (GIs) that have evolved for bacterial virulence, fitness, and adaptation to hosts and various environmental niches (2). However, existing biases in the G + C composition and codon usage of these GI genes impose transcription and translation limitations that may affect the physiology and fitness of bacterial hosts. Thus, the expression of GIs is tightly controlled by host regulatory networks (3–4). How bacteria discriminate themselves from foreign MGE DNA and offset the fitness costs of acquisition, amelioration, maintenance, and expression of these genes remains to be determined (3).

Nucleoid-associated proteins (NAPs) are small, basic, and highly abundant proteins that bind DNA, act as pivotal regulators of chromosome organization and play critical roles in facilitating or limiting the acquisition and expression of MGE DNA (5). Among a dozen NAPs encoded in *Escherichia coli*, H-NS is highly conserved and well characterized as an essential xenogeneic silencer (XS) that targets various AT-rich GIs by recognizing structural features unique to the minor groove of AT-rich DNA (6–8). H-NS

*To whom correspondence should be addressed. Tel: +86 21 64253306; Fax: +86 21 64253306; Email: oaiwqiyao@ecust.edu.cn
†The authors wish it to be known that, in their opinion, the first three authors should be regarded as Joint First Authors.

utilizes a "prokaryotic AT-hook motif" (Q/RGR) that inserts into the minor groove and forms extensive interactions along the groove floor (9). Global H-NS–DNA interactions alter nucleoid topology following folding into higher-order structures—i.e. superhelical nucleoprotein filaments—by wrapping, bending or bridging nucleic acids (5). Additionally, the cooperation between H-NS and other NAPs mediated by the spatial organization of their corresponding protein binding sites can further govern the higher-order architecture of the nucleoprotein complexes (10). Recent investigations have established that both chromosomally (endogenous) and MGE gene-encoded (xenogeneic) NAPs coexist in host bacteria (6,11–13). Although endogenous NAPs are well characterized in the xenogeneic silencing of MGE genes, including GIs and prophages, less is known concerning the roles of xenogeneic NAPs in their functional interaction with endogenous NAPs, in foreign element biology and in host cell physiology.

Edwardsiella bacteria are Gram-negative and zoonotic enteric bacterial pathogens that cause systemic infection in animals and humans (14). Among the several established species in the *Edwardsiella* genus, *E. piscicida* and *E. anguilarum* are the causative agents of edwardsiellosis for >20 species of piscine hosts, leading to huge economic losses in aquaculture worldwide (14,15). The *E. piscicida* genome harbours 24 horizontally acquired GIs (16,17), of which T3SS (GI7) and T6SS (GI17) have been established as pivotal for the bacterium to grow intracellularly and occupy the niche by translocating a repertoire of ∼20 putative and established effectors against host defences (14,18–20). T3SS in *E. piscicida* is analogous to the *Salmonella* pathogenicity island (SPI-2) in *S. Typhimurium* (15,21–22). In addition to the T3/T6SS gene clusters as in *E. piscicida*, *E. anguillarum* has acquired more GIs ($n = 33$), including the newly acquired locus of enterocyte effacement (LEE) genes (15).

GIs are tightly controlled by regulatory networks, as exemplified by the T3/T6SS in *E. piscicida* (14). The expression of T3SS and T6SS is controlled by several regulators, including the two-component system (TCS) EsrA-EsrB, which is homologous to SsrA-SsrB in *S. Typhimurium* (23) and essential for bacterial pathogenesis. Additionally, many other regulators, such as PhoP (24), RpoS (25) and EvrA (26), control T3/T6SS expression. Furthermore, H-NS has been established to control T6SS gene expression in *E. piscicida* (27–28). Using transposon insertion sequencing (TIS)-based technologies, a large compendium of genes essential for *in vivo* survival was revealed (19,26), warranting extensive exploration of their roles in modulating virulence programming *in vivo* and *in vitro* in the bacterium.

Here, we identified and characterized a novel regulator, EnrR, that resides in a GI harbouring MGE-associated genes and is closely related to the *in vivo* virulence of *E. piscicida.* EnrR controls T3/T6SS by competing with H-NS in the *esrB* promoter and derepressing its expression. EnrR colocalizes with bacterial nucleoid as an NAP. Structural analysis revealed a unique DNA binding mode of EnrR. Finally, this work revealed that EnrR can globally bind to and regulate GIs in *Edwardsiella* bacteria and *Salmonella*, controlling the expression of MGEs. Collectively, we show that EnrR is a unique NAP that plays a role as an H-NS-antagonizing virulence activator, providing insights into the mechanisms by which EnrR recognizes AT-rich DNA.

MATERIALS AND METHODS

Bacterial and cell strains, media and culture conditions

The bacterial strains and plasmids used in this study are listed in Supplementary Table S1. The *Escherichia coli*, *S. Typhimurium*, *E. piscicida* and *E. anguillarum* strains were cultured in Luria Bertani (LB) broth at 37 or 30°C. Notably, *E. piscicida* was grown statically at 30°C in DMEM for T3/T6SS production. *Escherichia coli* CC118 λ*pir* was used for plasmid preparation. Unless otherwise indicated, the plasmids were introduced into *E. coli* strains by transformation and into *E. piscicida*, *E. anguillarum* or *S. Typhimurium* by electroporation at 2000 V for 3 ms. When needed, ampicillin (Amp; 50 μg/ml), colistin (Col; 12.5 μg/ml), chloramphenicol (Cm; 34 μg/ml), streptomycin (Str; 100 μg/ml) and kanamycin (Kan; 50 μg/ml) were added.

Bacterial genetic engineering

The in-frame deletion mutants were generated by *sacB*-based allelic exchange as previously described (25). Briefly, upstream and downstream fragments were amplified by polymerase chain reaction (PCR) and then ligated into the suicide vector pDM4. The plasmid was transformed into SM10 λ*pir* and subsequently transferred into *E. piscicida*, *E. anguillarum* or *S. Typhimurium* by conjugation. The insertion mutants with single crossover recombination events were selected on LB agar medium containing Cm and Col, while double crossover recombination events were counterselected on LB agar medium containing 12% sucrose. An isogenic mutant with the wild-type *esrB* promoter (P_{esrB}) sequence replaced with mutant P_{esrB}lacking EnrR binding sites ($P_{esrB\text{mut1+2+3}}$) was similarly constructed. The respective complementation and overexpression plasmids were constructed with pUT as previously described (25).

Biofilm formation and autoaggregation assays

The biofilm formation ability of *E. piscicida* and *Salmonella* on polystyrene was quantified as described elsewhere (29–30). Briefly, bacteria were grown overnight in LB at 30°C. The cultures were diluted 1:100 in fresh LB, and 200 μl of the cell suspensions were statically subcultured into sterile 96-well polystyrene microtiter plates at 30°C for 24 h. Each well was washed with phosphate-buffered saline (PBS) three times. Next, total biofilm formation was measured using 2% crystal violet staining. Bacterial autoaggregation was observed after the cells were statically grown in DMEM at 30°C for 24 h (29).

Extracellular protein (ECP) assay

Overnight cultured bacteria were incubated in 5 ml of DMEM at 30°C for 24 h. Next, protease inhibitor (Roche, Switzerland) was added and incubated for 10 min at 4°C. After pelleting the cells at 5000 *g* for 10 min, the supernatants were filtered through a 0.22 μm low-protein-binding Millex filter (Millipore, USA) and concentrated to 250 μl using a 10-kDa-cut-off Amicon Ultra15 centrifugal filter (Millipore, USA). The concentrated ECP profile was detected by SDS-PAGE as previously described (25).

The supernatants of the same amounts of cells were also resolved by SDS-PAGE following silver staining.

Quantitative RT-PCR (qRT-PCR) and RNA-seq analyses

qRT–PCR and RNA-seq detection of gene transcripts were performed as described previously (23,25). *Edwardsiella piscicida* and *S. Typhimurium* were cultured in DMEM at 30 or 37°C for 12 h. Total RNA was extracted using an RNA isolation kit (Tiangen, China). For qRT-PCR, 1 μg of RNA from each sample was used to remove genomic DNA with DNase I (Promega, Madison, WI, USA), and reverse transcription was performed using the FastKing One Step RT-PCR Kit (Tiangen, China). Three independent qRT-PCR experiments were performed in triplicate using specific primer pairs (Supplementary Table S2) (Applied Biosystems, USA). RNA-seq was performed using a service provided by Personalbio China, and the sequencing data were analysed using Rockhopper (Version 2) as previously described (23,31).

Chromatin immunoprecipitation sequencing (ChIP-seq) and ChIP–qPCR

Δ*enrR* strains expressing EnrR-FLAG or FLAG alone driven by P_{enrR} in a plasmid were used for ChIP assays as previously described (25). Notably, bacteria were incubated in DMEM at 30°C for 12 h. The cultures were treated with 1% formaldehyde at room temperature for 10 min, and the reaction was stopped by adding 125 mM glycine. Next, the bacteria were washed twice with cold PBS and resuspended in 15 ml of IP buffer (50 mM HEPES-KOH pH 7.5, 0.1% sodium deoxycholate, 150 mM NaCl, 1 mM EDTA pH 8 and moderate protease inhibitor). High pressure and ultrasound were used to disrupt bacteria and for subsequent DNA fragmentation, respectively. The fragmented DNA was purified by phenol/chloroform and precipitated using a Dr GenTLE precipitation carrier (Takara, Japan). Next, the sequencing library was constructed using a VAHTS Turbo DNA library prep kit (Vazyme, China) and sequenced using the MiSeq platform (Illumina, USA). The sequencing data were analyzed using the MACS algorithm (32) and MEME analysis to generate the EnrR-binding motif (https://meme-suite.org/). KEGG pathway analysis was performed using Kobas 2.0 (33).

ChIP–qPCR analyses were performed as previously described to validate the binding of EnrR to the specific DNA motifs identified in the above-mentioned ChIP-seq assays (26). Briefly, *E. piscicida* strains chromosomally expressing EnrR-FLAG or FLAG alone in the *enrR* locus driven by native P_{esrB}were treated with ChIP followed by qPCR with various specific primer pairs (Supplementary Table S2) targeting the ∼100 bp central region in ChIP-seq peaks. For each DNA target, the ΔC_T values of the input and IP fractions were calculated in both samples for the EnrR-FLAG- and FLAG-expressing strains. Each value was then divided by the corresponding ΔC_T of the nonspecific *gyrB* promoter region in the strains. Next, the enrichment ratio was calculated using the $\Delta\Delta C_T$ value in the EnrR-FLAG strain divided by that of the FLAG strain. The ChIP–qPCR assays of H-NS binding to specific gene promoters were performed similarly using the anti-GST magnetic beads (Beyotime, Shanghai).

Lysogeny phage-related experiments

Bacteria were fixed in 2.5% glutaraldehyde in PBS for 12 h at 4°C, dehydrated with a series of gradient ethanol solutions (30–100%) and freeze-dried. Subsequently, the samples were coated with gold film by sputter coating and then observed under a field emission scanning electron microscope (S3400-N; Hitachi, Japan). Phages released from the bacteria were extracted using the Universal Phage Genomic DNA Extraction Kit (Knogen Biotech, China). Phage particles were resuspended in SM buffer (100 mM NaCl, 8 mM $MgSO_4{\cdot}7H_2O$, 50 mM Tris-Cl pH 7.5; 0.002% w/v gelatine) and negatively stained with 2% phosphotungstic acid for 10 min followed by observation under a transmission electron microscope (JEM-1400; JEOL, Japan).

Purification of protein

The expression of C-terminal-tagged EnrR or N-terminal-tagged H-NS was induced by 0.2 mM isopropyl β-D-1-thiogalactopyranoside (IPTG) in *E. coli* BL21 (DE3) at 20°C at 120 rpm. At 18 h postinduction, the bacteria were harvested by centrifugation and purified as previously described (25).

Electrophoretic mobility shift assay (EMSA), bacterial one-hybrid (B1H) assay and microscale thermophoresis (MST) analyses

EMSA and B1H assays were conducted as previously described (30). To measure the protein affinity to a specific DNA probe, Cy5-labelled DNA was used, and the purified protein was diluted with TE buffer (10 mM NaCl, 0.5 mM EDTA, 10 mM Tris-HCl pH 7.5) followed by mixing protein and DNA at a volume ratio of 1:1. For MST assays of EnrR or H-NS affinities to specific DNA probes, EnrR or H-NS was labelled with RED-tris-NTA dye (MO-L018; Nano Temper, Germany) and then was mixed with an equal volume of the diluted DNA probes. After incubation for 20 min at room temperature, a Monolith NT™ capillary (Nano Temper, Germany) was horizontally placed into the reaction tube to aspirate the sample, and thermophoresis was detected using a Monolith NT.115 system (Nano Temper, Germany).

DNA-protection assay

DNA-protection assays were performed as previously described (34). Notably, a series of concentrations of EnrR (0–16 μM) were incubated with 750 bp P_{2212}-*750* DNA (200 ng of the promoter region of ETAE_2212) for 30 min at room temperature in TE buffer. Next, 20 μl of the mixture was treated with 0.5 U of DNase I (NEB, UK) for 5 min at 37°C. The reactions were terminated by incubation at 70°C for 10 min, followed by treatment with proteinase K (20 μg), 5 mM $MgCl_2$, 2% SDS and 0.3 M sodium acetate for 1 h at 37°C. The samples were extracted using phenol/chloroform and precipitated using a Dr. GenTLE

precipitation carrier (Takara, Japan). The pellets were dissolved in 10 μl of ddH_2O and run on a 1% agarose gel in TAE at 100 V for 30 min.

Plasmid supercoiling conformation assay

The supercoil assay was performed according to a previously published procedure using freshly prepared pUT plasmid (35). The plasmid was incubated with various amounts of EnrR at 37°C for 30 min. Next, topoisomerase I (TopA) (Takara, Japan) was added to the mixtures and incubated at 30°C for 30 min. The reaction was subsequently terminated by proteinase K (20 μg). The samples were analysed by 1% agarose gel electrophoresis.

Fluorescence colocalization assays

An *E. piscicida* strain expressing the EnrR-GFP fusion protein driven by the P_{enrR} promoter at the *enrR* locus was constructed. After 6 h of growth, the bacteria were washed twice with cold PBS and stained with DAPI for 30 min on LBA. The samples were visualized by differential interference contrast (DIC) and fluorescence microscopy using a confocal microscope (A1R; Nikon, Japan).

Atomic force microscopy (AFM)

The circular pUT vector or linear P_{2212}-*750* DNA was incubated with different concentrations of EnrR protein in TE buffer at room temperature for 30 min. A 10 μl droplet of the mixtures was placed onto fresh mica for 2 min. Next, the mica was rinsed with Milli-Q water and dried under a stream of nitrogen. The samples were visualized by scanning probe microscopy (Veeco, USA).

Crystallization and data collection

Both native and Se-substituted EnrR proteins in gel filtration buffer were concentrated to 10–12 mg/ml. To prepare the DNA complex, EnrR and DNA1 were mixed at a molar ratio of 1:1.2 and incubated at room temperature for 30 min. The crystallization conditions were initially identified at 16°C using crystallization kits from Hampton Research Company and a crystallization robot system using the sitting-drop vapour diffusion method at 0.4 μl per drop (1:1 ratio of protein–DNA mixture or protein alone to well solution). Crystallization was optimized using the hanging-drop vapour diffusion method. Apo-EnrR crystals were grown in 20% PEG 3350 and 0.2 M sodium formate. EnrR-DNA1 complex crystals were grown in 20% PEG 3350 and 0.2 M K_2SO_4 buffer supplemented with 0.2 M D-sorbitol. Crystals of apo-EnrR were cryoprotected using their mother liquor supplemented with 25% glycerol, whereas EnrR-DNA1 complex crystals were cryoprotected using 30% PEG 400. All the crystals were snap-frozen in liquid nitrogen. X-ray diffraction data (Table 1) were collected on beamlines BL17U and BL19U at the Shanghai Synchrotron Radiation Facility (SSRF). Data processing was performed using the HKL2000 or HKL3000 programs (36).

Table 1. Data collection and refinement statistics

Structure (PDB ID)	Apo-EnrR 7F9I	EnrR/DNA1 7F9H
Data collection[a]		
Space group	$P2_12_12_1$	C2
Cell parameter		
a, *b*, *c* (Å)	34.1, 56.3, 72.4	104.3, 58.5, 67.6
α, β, γ (°)	90.0, 90, 90.0	90.0, 98.4, 90.0
Wavelength (Å)	0.9793	0.9793
Resolution (Å)	30.0–2.5	30.0–1.75
Highest resolution shell (Å)	2.59–2.50	1.84–1.75
Completeness (%)	97.2(93.2)	98.1(67.0)
Redundancy	6.1(4.2)	6.7(6.0)
I/σ(I)	10.1(2.7)	26.2(4.8)
R_{merge} (%)	14.3(38.2)	5.4(38.3)
Refinement		
Resolution (Å)	28.1–2.5	29.6–1.78
R_{work} (%)/R_{free} (%)	24.5/28.2	20.1/22.2
No. of atoms		
Protein	1061	1164
DNA	0	898
Water	2	228
Wilson B factors (Å^2)	19.3	17.6
R.m.s. deviations		
Bond length (Å)	0.012	0.007
Bond angles (°)	1.492	1.309
Ramachandran plot (%)		
Most favoured	96.2	97.1
Additional allowed	3.8	2.9

Structure determination and refinement

The phases of the Se-substituted EnrR-DNA1 complex structure were determined using the single-wavelength anomalous diffraction (SAD) method (37) and the anomalous signal of Se- atoms with the AutoSol program (38) embedded in the Phenix suite (39). The initial model was refined using the Refmac5 program (40) of the CPP4i suite (41). The apo-EnrR structure was solved using the molecular replacement method; the EnrR molecule of the complex was used as a search model. The model was manually built using COOT (42) and refined using either Refmac5 or phenix.refine programs (43). During refinement, 5% of randomly selected data were set aside for free R-factor cross-validation calculations. The 2Fo–Fc and Fo–Fc electron density maps were regularly calculated and used as guides to build the missing amino acid residues and solvent molecules with COOT. The structural refinement statistics are summarized in Table 1.

Animal survival, *in vivo* competition and luminescence assays

Fish-related experiments were performed as previously described (25). Briefly, 3-month-old healthy turbots weighing approx. 25 ± 3 g were used for the experiments. Fish were anaesthetized (10 min) in sea water supplemented with MS-222 (0.02% v/v) (Sigma-Aldrich) and aseptically dissected to harvest their tissues. For survival assays, different concentrations of bacteria (2×10^2–10^3 CFU/g) were inoculated into fish at 100 μl intraperitoneally (i.p.), and fish survival was monitored over 30 days.

For *in vivo* competition assays, the paired bacterial strains were resuspended and mixed 1:1 in PBS. Next, the mixtures were diluted and i.p. injected into fish at a dose of

3×10^5 CFU/fish, and fish tissues were harvested at 5 days post-infection (DPI) when *E. piscicida* established colonization and systemic infection (19,25). The cell-forming units (CFU) per gram of tissue were enumerated by plating homogenized tissue on DHL agar containing appropriate antibiotics.

For *in vivo* luminescence detection, the subcultures of reporter strains were diluted to 10^6 CFU/ml in PBS and i.p. injected into turbot at 100 μl. At 5 DPI, the fish were i.p. inoculated with beetle luciferin substrate (Promega). After 10 min, the fluorescence was detected using the Kodak In-Vivo Multispectral System FX (Carestream Health) as previously described (25). Next, the livers of the fish were sampled, and bacterial colonization was enumerated by CFU plating.

Ethics statement

All the animal protocols used in this study were approved by the Animal Care Committee of the East China University of Science and Technology (2006272). The Experimental Animal Care and Use Guidelines from the Ministry of Science and Technology of China (MOST-2011-02) were strictly followed.

RESULTS

EnrR is a new virulence regulator crucial for *E. piscicida* infection *in vivo*

To identify genes temporally required for *E. piscicida in vivo* survival in hosts, we devised and applied the algorithm termed pattern analysis of conditional essentiality (PACE) to time series transposon insertion sequencing (TIS) data collected during a 14-day *in vivo* infection experiment in a turbot infection model (19). Because T3SS and T6SS have been established as key determinants during the progression of *E. piscicida in vivo* infection (19,25–26), we compared genes with similar *in vivo* essentiality patterns to those of the T3SS or T6SS loci—e.g. *esrB*, *eseB* and *evpP*—from the PACE analysis of the TIS dataset (19). Thus, we identified that the mutant of ETAE_0051 (hereafter referred to as *Edwardsiella* nucleoid-associated regulator R, *enrR*) showed a normalized median fitness decrease of approximately -0.25 $\log_2$-fold change (FC) per day, comparable to that of T3/T6SS insertion mutants, indicating its attenuation in its colonization capacities *in vivo* (Figure 1A).

The *enrR* gene is localized in *E. piscicida* GI2, flanked by genes encoding transposases, integrases and DNA repair proteins as well as clustered genes encoding uncharacterized phage-like proteins (Figure 1B) that appear to be horizontally acquired from decayed prophages and are present in various phylogenetically distant bacteria (Supplementary Figure S1). Bioinformatics analysis showed that the *enrR* gene encodes a hypothetical small regulatory protein of 90 amino acid (aa) residues with a winged helix-turn-helix (w-HTH) DNA-binding domain (PF13693) that belongs to the XRE superfamily (Figure 1C). To verify the *in vivo* TIS results, the *enrR* in-frame deletion mutant strain Δ*enrR* and its complement strain Δ*enrR*$^+$ were constructed. The Δ*enrR* strain showed no growth difference from the wt strain when grown in either DMEM or LB medium (Supplementary Figure S2A,B). Compared with the wt strain, the Δ*enrR* strain showed drastically impaired virulence and caused significantly lower mortalities in turbot, a natural host (16), over 24 days post-infection (DPI) (Figure 1D). Introduction of the *enrR* gene into the Δ*enrR* mutant strain restored its infectivity in a fish model. These results indicated that *enrR* is essential for bacterial virulence towards hosts.

EnrR controls T3/T6SS expression *in vitro* and *in vivo*

To clarify the roles of EnrR in bacterial virulence, we examined whether the control of virulence by EnrR is related to T3/T6SS expression. First, we tested wt-, Δ*esrB*- and *enrR*-related strains using an assay of autoaggregation, a phenotype attributable to the production of the T3SS extracellular apparatus protein EseB (29), and extracellular protein (ECP) profiling by SDS–PAGE analysis (Supplementary Figure S2C,D). As expected, the Δ*enrR* strain and complement strain *enrR*$^+$ showed patterns of autoagglutination and EseB production similar to Δ*esrB* and its complementation strains, respectively (Figure 2B). Western blot analysis of T3/T6SS secretion using the antiserum against the T3SS protein EseB and T6SS protein EvpP further confirmed that EnrR positively regulates T3/T6SS production (Figure 2B, bottom). Similar to the above analyses, qRT-PCR also showed that T3/T6SS gene transcripts were upregulated by EnrR (Figure 2C).

Subsequently, we investigated the *in vivo* involvement of EnrR in T3/T6SS expression during infection in a fish model. Competitive index (CI) experiments were performed in which Δ*enrR*, Δ*eseBCD*, Δ*evpAB* and the Δ*enrR*Δ*eseBCD* and Δ*enrR*Δ*evpAB* mutant strains were mixed equally with WTΔp, the wt strain cured with pEIB202. The CI results at 5 DPI showed that the Δ*enrR* strain was significantly ($P < 0.01$) impaired in fitness in fish (Figure 2D) and comparable to that of T3SS- or T6SS-related mutants, further corroborating the idea that EnrR controls T3/T6SS expression. Next, *in vivo* bioluminescence imaging was used to investigate EnrR regulation of T3/T6SS during *E. piscicida* infection of turbot. Luciferase reporters of P_{eseB}- and P_{evpA} expression were introduced into a neutral position on the chromosomes of the wt and Δ*enrR* strains, respectively, and these strains were intraperitoneally (i.p.) inoculated into turbot fish at the same dose. At 5 DPI, significantly decreased P_{eseB}- and P_{evpA}- activity was detected in the Δ*enrR* strain background compared with that in the wt strain (Figure 2E). Taken together, these results revealed that EnrR controlled T3/T6SS expression *in vitro* and *in vivo* during infection.

EnrR regulates *E. piscicida* virulence via EsrB

The response regulator EsrB is pivotal for the expression of T3/T6SS in *E. piscicida* (25). We reasoned that EnrR controls *E. piscicida* T3/T6SS expression by modulating *esrB* expression because *esrB* overexpression driven by the promoter for the 30S ribosomal protein ETAE_0456 (P_{0456}) in the Δ*enrR* strain could restore the autoaggregation phenotype and T3/T6SS production (Figure 2A,B), and the transcript level of *esrB* was downregulated in the Δ*enrR* strain

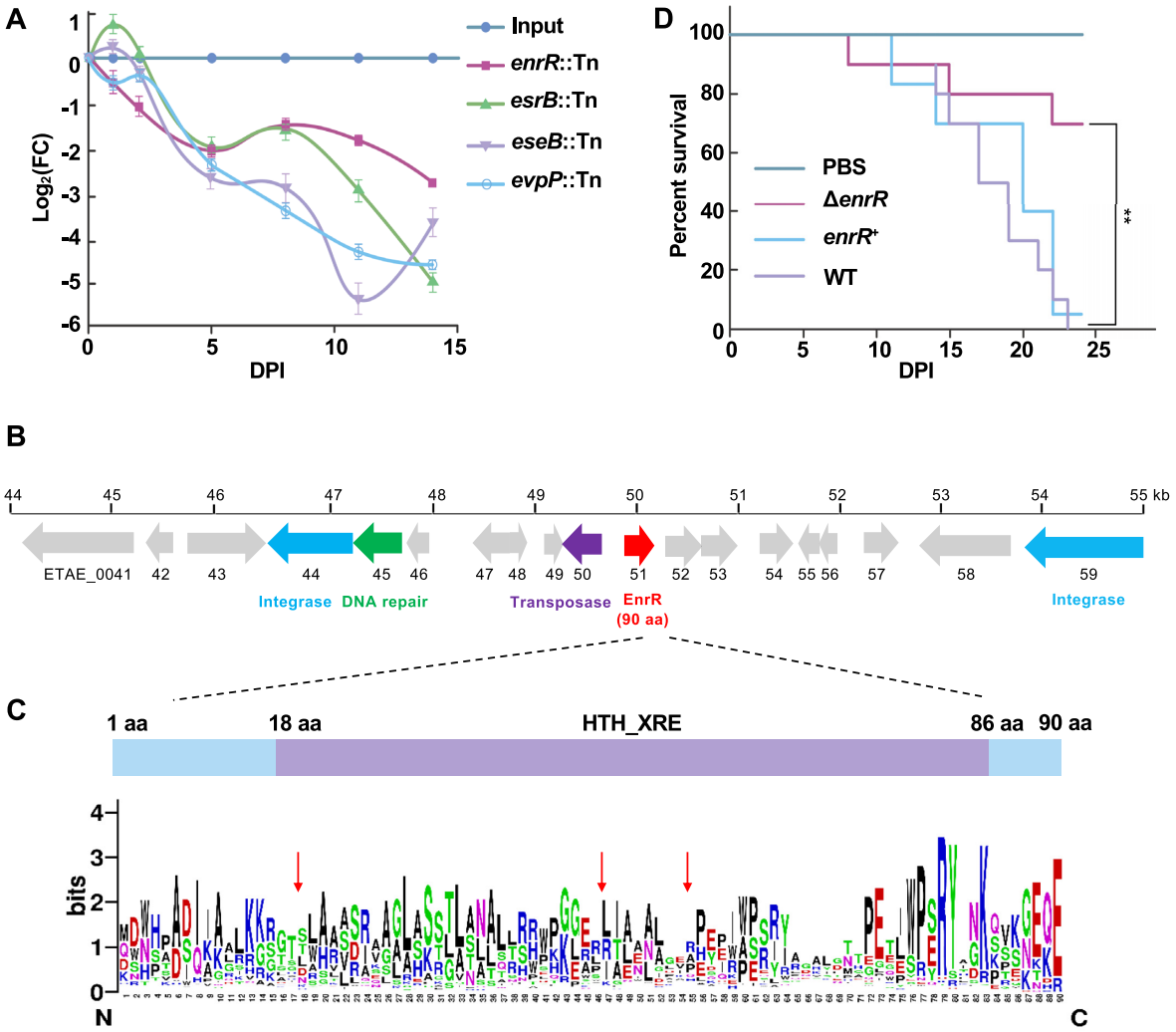

Figure 1. Characterization of the *enrR* mutant. (**A**) Relative *in vivo* fitness profiles of transposon (Tn) insertion mutants of ETAE_0051 (*enrR*), *esrB*, *eseB* and *evpP*. The dynamic log2-fold change (FC) in abundance for each mutant strain recovered from the liver relative to the wt strain was plotted against the days postinjection (DPI) by intraperitoneal (i.p.) injection of a highly saturated mutant library in turbot. (**B**) The gene locus of ETAE_0051 (*enrR*) neighbours the MGEs. (**C**) Structural analysis of EnrR. Red arrows represent the residues that recognize specific nucleobases. Larger letters represent more conservative residues. (**D**) Survival curve of turbot fish challenged with wt and Δ*enrR* strains, as well as the Δ*enrR* strain harbouring the complement plasmid pUT-*enrR* (*enrR*$^+$) by i.p. injection ($n = 30$ per group). **, $P < 0.01$ by comparing the Δ*enrR* strain with the wt and *enrR*$^+$ strains using Kaplan–Meier survival analysis using the log rank test (Mantel–Cox).

(Figure 2C). Next, we performed genetic analysis of *esrB* in mediating the EnrR control of T3/T6SS expression in various genetic backgrounds of *E. piscicida* EIB202 and *E. anguillarum* ET080813, a strain that encodes T3/T6SS GIs and the EsrA-EsrB two-component system but does not encode *enrR* homologue (15). In EIB202, the introduction of P_{0456}-driven *enrR* and *esrB* or *esrB* encoding the D60E variant (*esrB*^{D60E}) mimicking constitutive phosphorylation in EsrB fully restored the T3/T6SS production defects in the Δ*enrR* strain (Figure 2F, lanes 5–7), although *esrB* or *esrB*^{D60E} showed similar capacities in activating T3/T6SS production, likely because of sufficient phosphorylation for EsrB. Additionally, the expression construct P_{0456}-*esrB*, but not P_{0456}-*enrR*, activated T3/T6SS expression in the Δ*enrR*Δ*esrB* double mutant (Figure 2F, lanes 8 and 9), indicating that EnrR is epistatic to EsrB with respect to the T3/T6SS regulatory pathway. This notion was also supported by the result observed in ET080813, in which T3/T6SS production could be triggered by introducing an *enrR* overexpression plasmid (Figure 2F, lanes 10 and 11). The process was EnrR- and EsrB dependent because neither the expression of a DNA-binding mutant of EnrR, EnrR^{R47G} in the wt strain, nor the Δ*esrB* mutant strain containing the *enrR* overexpression plasmid showed wt levels of T3/T6SS (Figure 2F, lanes 12 and 13). Notably, the crystal structure (to be described later) revealed that the R47 residue was essential for the DNA binding of EnrR.

Next, we asked whether the control of the *esrB* promoter activity by EnrR was associated with T3/T6SS production. In EIB202, the expression of *esrB* driven by both the native *esrB* promoter (P_{esrB}) and P_{0456} fully restored T3/T6SS expression in the Δ*esrB* strain (Figure 2G, lanes 3 and 4). However, in the ET080813 background, these two expression constructs could not generate T3/T6SS production al-

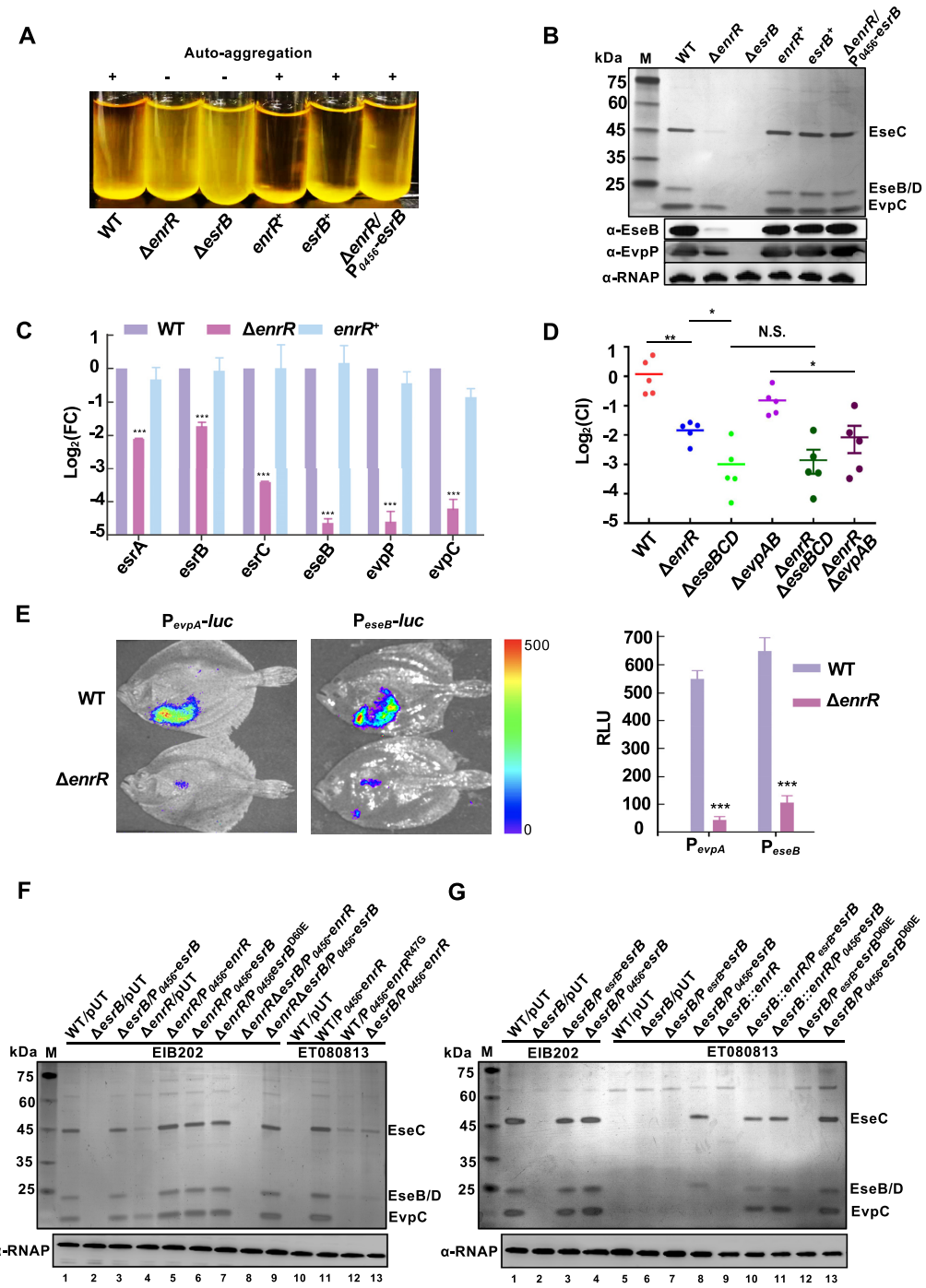

Figure 2. EnrR is a positive regulator of virulence *in vitro* and *in vivo* and functions by regulating *esrB*. (**A** and **B**) Autoaggregation (A) and extracellular protein (ECP) profiles (B) of the indicated strains statically cultured in DMEM. The supernatants from the same amounts of cells were resolved by SDS–PAGE and silver stained (upper panel), and specific bands corresponding to T3SS and T6SS proteins are shown. The SDS–PAGE-resolved proteins were then blotted with anti-EseB- or anti-EvpP-specific antiserum (lower panels). RNAP was used as the loading control for the blots. (**C**) qRT–PCR assays for the indicated transcripts in the wt, Δ*enrR* and *enrR*$^+$ strains. The results shown are the means ± S.D. ($n = 3$) relative to the wt results. *gyrB* was used as the internal control. ***, $P < 0.001$ compared with wt based on Student's *t*-test. (**D**) *In vivo* competition assays of the equally mixed indicated strains (Cm resistance) and WTΔp, the wt strain with pEIB202 cured (Cm sensitive) inoculated into fish and recovered from the livers of turbot fish at 8 DPI ($n = 5$ per group). ** $P < 0.01$, * $P < 0.05$ and N.S. (not significant) for $P > 0.05$, based on one-way ANOVA and Fisher's LSD multiple comparison post-test. (**E**) Activities of the promoters of *evpA* and *eseB* from T3/T6SS gene loci in wt or Δ*enrR* strains inoculated *in vivo* in fish. The indicated strains harbouring P_{evpA}-*luc* or P_{eseB}-*luc* reporter plasmids were inoculated into turbot, and bioluminescence was measured at 8 DPI and normalized by CFU. ***, $P < 0.001$ based on ANOVA of the relative fluorescence units (RFU). (**F** and **G**) EnrR regulates T3/T6SS gene expression through *esrB* in both *E. piscicida* EIB202 and *E. anguillarum* ET080813 strains. The wt, Δ*esrB* or Δ*enrR* strains of EIB202 or ET080813 harbouring the empty vector pUT or the plasmid expressing *esrB* or *enrR* driven by their respective promoters—i.e. P_{esrB} or P_{enrR} or by the constitutive promoter for the 30S ribosomal protein (P_{0456})—were investigated for their production of T3/T6SS proteins in the ECPs by SDS–PAGE.

though P_{0456}-*esrB* caused minimal T3/T6SS proteins in the Δ*esrB* strain (Figure 2G, lanes 7 and 8). We used the expression of $esrB^{D60E}$ driven by P_{esrB} or P_{0456} in Δ*esrB* to minimize the effect of upstream phosphorylation by the cognate histidine kinase EsrA, and only the latter triggered the wt EIB202 level of T3/T6SS expression (Figure 2G, lanes 12 and 13). These results suggested that the activity of P_{esrB} could be regulated by a specific repressor in ET080813. Furthermore, compared with the Δ*esrB* strain chromosomally expressing EnrR—i.e. the Δ*esrB*::*enrR* strain, which showed deficiency in T3/T6SS production—the introduction of the plasmids expressing EsrB driven by P_{esrB} or P_{0456} fully augmented T3/T6SS expression (Figure 2G, lanes 9–11). The restoration of T6SS protein EvpC secretion in Δ*esrB*::*enrR* harbouring plasmid P_{0456}-*esrB* compared with the strain Δ*esrB*/P_{0456}-*esrB* suggested that EnrR might derepress *esrB* and another T6SS-related promoter (lanes 8 and 11). Collectively, these data demonstrated that EnrR controls T3/T6SS expression in *Edwardsiella* bacterium primarily by modulating *esrB* promoter activation.

Edwardsiella piscicida T3SS and its regulatory mechanisms are analogous to those of *S. Typhimurium* SPI-2. Expression of EnrR in *S. Typhimurium* SL1344, a strain that does not encode an EnrR homologue, resulted in higher levels of the SPI-2 transcript (Supplementary Figure S3A,B) and biofilm formation (Supplementary Figure S3C) than that of the control strain harbouring the empty plasmid. EnrR regulated SsaJ expression dependent on SsrB, the known master regulator of SPI-2 (Supplementary Figure S3B) (44–45). Compared with the Δ*ssrB*::pUt and Δ*ssrB*::pUt-*enrR* strains, all of the mice challenged with the EnrR-producing wt strain lost body weight and died in 7 days, while most (75%) of the mice injected with the same dose of the wt strain were still alive after 12 days (Supplementary Figure S3D,E). Taken together, these results showed that EnrR activated the expression of SPI-2 and enhanced *Salmonella* virulence through SsrB.

EnrR competes with H-NS from the *esrB* promoter to activate virulence gene expression

H-NS represses the transcription of T6SS genes in *Edwardsiella* bacteria (27–28). Here, we confirmed that H-NS overexpression inhibited the production of T3/T6SS proteins and EsrB in the wt and Δ*enrR* strains (Figure 3A, lanes 2 and 4, and Supplementary Figure S2E). Notably, H-NS is an essential gene in *E. piscicida* (19,26); its deletion mutant could only be generated with another repressor mutation, including *rpoS* null mutation, as described in other bacteria (3,8). Deletion of *hns* in the Δ*rpoS* context resulted in no obvious changes in the level of T3/T6SS proteins (Figure 3A, lanes 5–6), and the additional disruption of *enrR* in the Δ*hns* mutant led to marginally reduced T3/T6SS production (lanes 6 and 8). By contrast, *enrR* overexpression augmented the expression of these virulence genes in the presence or absence of *hns* (lanes 9–10). Thus, these data suggested a role of EnrR in overcoming H-NS inhibition of *esrB* expression, although we could not exclude the activity of EnrR as a transcriptional activator.

We then investigated whether EnrR and H-NS could directly bind to the promoter region of *esrB* using MST analyses. EnrR and H-NS could bind to P_{esrB} with dissociation constants (K_d) of 11.5 ± 0.4 μM and 18.1 ± 2.8 μM, respectively (Figure 3B). EMSA experiments and B1H also demonstrated the binding ability of EnrR with P_{esrB} (Supplementary Figure S4A,C) (30). Furthermore, dye primer-based DNase I footprinting assays mapped at least three AT-rich binding sites of EnrR (Figure 3C) and two binding regions of H-NS (Figure 3D) just upstream of the *esrB* promoter region (Figure 3E). Distinct mutations in these regions (mut1-mut3 and mut1 + 2 + 3 for EnrR, mut4-mut5 and mut4 + 5 for H-NS) resulted in various extents of decrease in the affinities of these two proteins to the target probes (Figure 3B). Additionally, EnrR did not appear to bind with H-NS under *in vitro* conditions (Supplementary Figure S4F). Collectively, these analyses demonstrated that both EnrR and H-NS could bind to the *esrB* promoter region.

MST assays intriguingly revealed that the DNA binding of H-NS to P_{esrB} was significantly reduced in the presence of EnrR (Figure 3B). To further determine whether EnrR competed with H-NS from the *esrB* promoter *in vitro*, we performed EMSA using both GST-H-NS and His_6-EnrR (or otherwise the null mutant His_6-$EnrR^{R47G}$) added to *esrB* promoter DNA (Figure 3F). The GST- or His_6-tagged H-NS or EnrR behaved similarly to their wt proteins in the control of T3/T6SS production (Supplementary Figure S2D). EMSA confirmed that their binding to P_{esrB}increased with increasing protein concentrations (0–3 μM), and many more oligomerized protein–DNA complexes for H-NS were found than for EnrR (Figure 3F, left column). When a constant amount (3 μM) of H-NS was added, increasing concentrations (0.5–6 μM) of EnrR resulted in enhanced shifts for the migration of the nucleoprotein complex, similar to that of the EnrR-P_{esrB} complex (Figure 3F, right column). This analysis suggested that EnrR competed with H-NS from this promoter DNA. The proteins in EMSA gels were then transferred to a PVDF membrane to determine whether any H-NS protein remained bound to the shifted DNA substrate via Western blotting. As expected, as the EnrR concentration increased from 0.5 to 6 μM across reactions and the signal corresponding to unbound H-NS accumulated (Figure 3F, right column, lanes 4–7). Additionally, the parallel increase in $EnrR^{R47G}$ from 2 to 6 μM could not prevent the DNA binding of H-NS and remove it from P_{esrB} (Figure 3F, right column, lanes 8–10). These results confirmed that EnrR antagonization of H-NS relied on EnrR-DNA binding activity.

We further investigated the effects of H-NS occupancy on the *esrB* promoter in cells grown under T3/T6SS induction conditions. The *hns* gene is highly conserved and self-controlled in *E. coli* and other bacteria (7). Using ChIP–qPCR assays, we determined that H-NS bound to the *esrB* promoter region more strongly in the strain with the mutant P_{esrB} lacking the identified EnrR binding sites (Figure 3C,E) than in the isogenic wild-type P_{esrB}strain (Figure 3G). Control experiments showed that the strain with the $P_{esrB\text{mut1+2+3}}$ mutation retained normal H-NS binding to the *hns* DNA (Figure 3G) and extremely low binding to the DNA region upstream of *gyrB* (Figure 3G). In summary, these findings demonstrated that EnrR antagonized H-NS binding to the *esrB* promoter region and alleviated H-NS

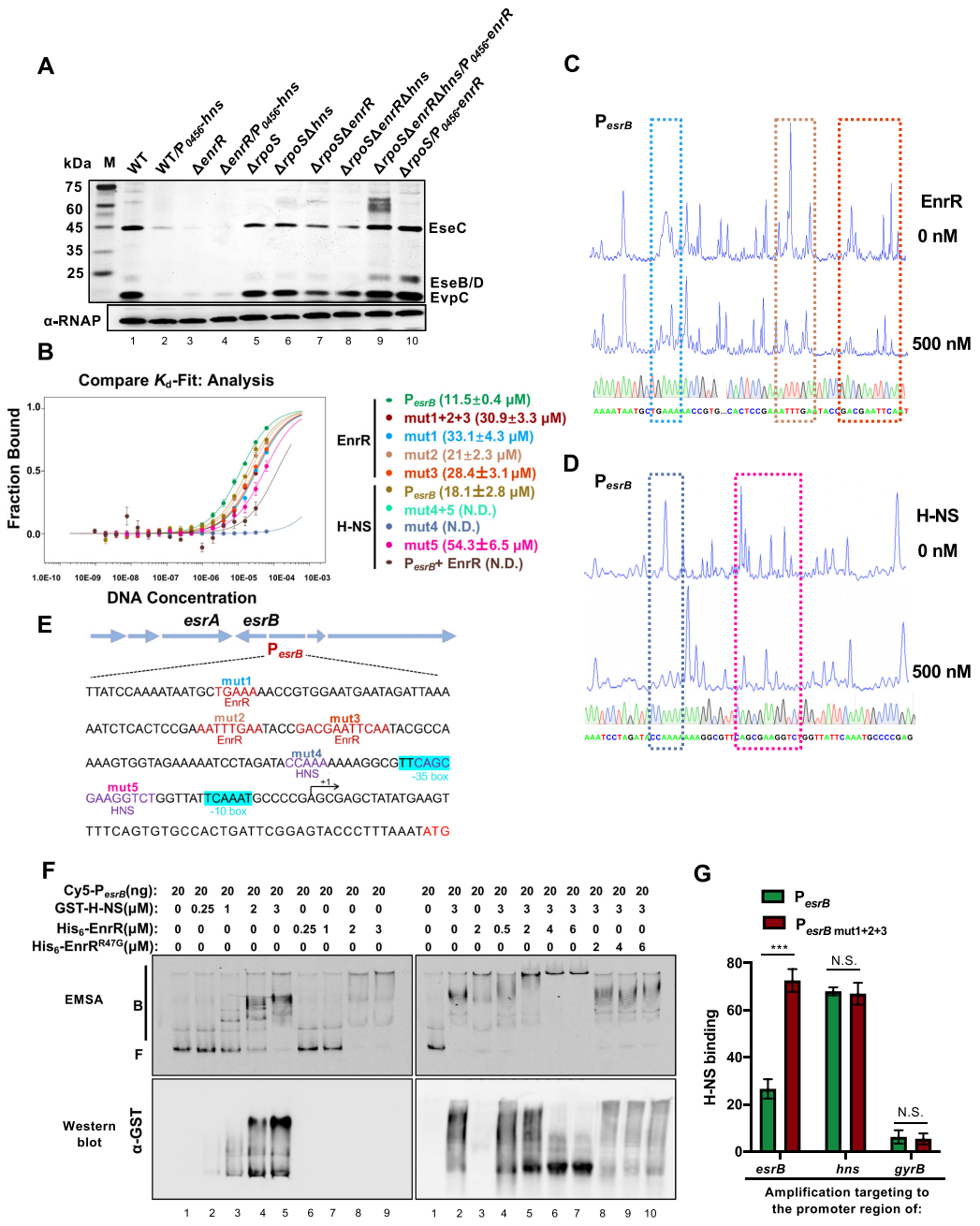

Figure 3. EnrR binds to the *esrB* promoter region and antagonizes H-NS binding. (**A**) SDS–PAGE analysis of the ECPs from the indicated wt or Δ*enrR* strains overexpressing H-NS or with *hns* deletion in the Δ*rpoS* context. Note that *hns* is an essential gene that can only be disrupted in the presence of additional *rpoS* suppressor mutations. (**B**) MST analysis of EnrR or H-NS binding to *esrB* promoter DNA (P_{esrB}) probes. Purified EnrR and/or H-NS protein was labelled with RED-tris-NTA dye and then incubated with wt or mutant P_{esrB} probes of increased concentrations in NT standard capillaries in MST assays. The *y*-axis represents the fractions of proteins being bound. The *x*-axis is the mol concentration per litre of DNA. The curve is the fit of data points to the standard K_d-fit function. The respective K_d (dissociation constant) values from triplicate assays are shown as means ± S.D. in brackets. Note that the data points of the P_{esrB} mut4 + 5 probe could not fit into a curve. N.D., not detectable. (**C** and **D**) DNase I footprinting analysis of EnrR or H-NS binding to P_{esrB} DNA. Electropherograms of a DNase I digest of the P_{esrB} promoter probe after incubation with or without EnrR (C) and H-NS (D). The respective nucleotide sequences protected by the proteins are boxed in colours. (**E**) Diagram of the P_{esrB} region. The EnrR- or H-NS-protected regions, -10 and -35 boxes for RNAP binding and the transcriptional and translational start sites are highlighted. The probes with mutated regions for binding assays are shown as mut1-mut5, mut1 + 2 + 3, or mut4 + 5 (B). (**F**) H-NS competes with EnrR for binding to P_{esrB} DNA *in vitro*. Top panel, EMSAs containing Cy5-labelled P_{esrB} DNA and either purified GST-tagged H-NS or His_6-tagged EnrR or $EnrR^{R47G}$. Competitive EMSA reactions comprising 3 μM purified H-NS, and either 0.5, 2, 4 or 6 μM purified EnrR are shown in the top right. The reactions were run on polyacrylamide gels and laser scanned at 650 nm. B: bound DNA; F: free DNA. Bottom panel, the gels were then transferred to a PVDF membrane and probed for H-NS using anti-GST antibodies. (**G**) *In vivo* binding of H-NS to the promoter regions of the *esrB*, *hns* and *gyrB* genes was determined in GST-H-NS-expressing *E. piscicida* cells harbouring wt or mutant P_{esrB} or $P_{esrB\text{mut1+2+3}}$ grown in DMEM for 12 h using ChIP with anti-GST magnetic beads. The relative enrichment of GST-H-NS on P_{esrB}, P_{hns} and P_{gyrB} DNA was subsequently assayed by qPCR experiments with primer pairs targeting these regions. ***, $P < 0.001$, N.S., $P > 0.05$ based on Student's *t*-test of the relative H-NS binding enrichments normalized to that of *rpoD* ($n = 3$).

repression of the master regulator EsrB to promote virulence gene expression.

EnrR features NAP protein binding to DNA *in vivo* and *in vitro*

EnrR is a small, basic (PI = 11.4), and highly expressed DNA-binding protein with an estimated ∼29 000 copies per cell (Supplementary Figure S2H) comparable to the H-NS abundance and is hypothesized to be an NAP. To test this hypothesis, we first characterized the DNA-binding properties of EnrR. EnrR could specifically and widely protect against DNase I digestion treatment of the 750 bp DNA probe of the promoter region of ETAE_2122 (Figure 4A) that was enriched by ChIP-seq analysis (see below). Further evaluation of the *in vitro* effect of EnrR on the activity of bacterial topoisomerase TopA showed that the plasmid DNA relaxed by TopA gradually transformed to a supercoiled configuration with increasing concentrations of EnrR (Figure 4B), indicating EnrR's inhibitory function against the DNA relaxation activity of TopA. By contrast, BSA protein showed no resistance to the DNA relaxation activity of TopA. In the DNA-binding competition experiments, the amount of EnrR-DNA complex decreased with increasing concentrations of actinomycin D or methyl green, the specific minor- and major-groove binding drugs, respectively (Figure 4C) (34), strongly suggesting that EnrR could bind to the DNA minor and major grooves.

Using an atomic force microscopy (AFM) assay, we further characterized EnrR-DNA complexes and the structural effects of EnrR on both 750 bp DNA fragments (Supplementary Figure S6) and circular plasmid DNA (Figure 4D). The addition of increasing concentrations of EnrR protein led to DNA oligomerization or aggregation into larger globular particle complexes on the mica surface (Supplementary Figure S5A-D), a finding that was consistent with the observation that the EnrR-DNA complex was blocked in the loading well during EMSA experiments (Figure 4C and Supplementary Figure S4A,B). As a control, a high concentration (16 μM) of $EnrR^{R47G}$ showed defects in forming globular particles with the DNA (Supplementary Figure S5E). Compared with the uniform protein-free structure of DNA, the mixture of EnrR and plasmid DNA resulted in the condensation of the proteins along the DNA contour. In particular, some EnrR-rich cores were observed around the DNA loops/bridges (Figure 4D).

A subsequent colocalization experiment was performed to determine whether EnrR localizes to bacterial genomic DNA. A functional green fluorescence protein (GFP)-fused recombinant EnrR protein (Supplementary Figure S2D) was produced in *E. coli* with a plasmid or chromosomally expressed in the native *enrR* locus in *E. piscicida*, and the bacterial nucleoid was stained with DAPI (Figure 4E and Supplementary Figure S5G). The GFP fluorescence signals closely coincided (Pearson's rho [*R*r] > 0.9) with the DAPI-stained regions, demonstrating that EnrR colocalizes with the bacterial nucleoid (Figure 4E and Supplementary Figure S5G). Collectively, these results revealed that EnrR can broadly bind to different regions of DNA, plasmids and the nucleoid. Thus, we propose that EnrR represents a newly described NAP.

EnrR globally binds to and regulates genes involved in various processes

Next, we investigated whether other genes and processes are regulated by EnrR, which would be conducive to virulence and adaptation in host niches. We used ChIP-seq to determine the EnrR regulon (Supplementary Table S3). We used the Δ*enrR* strain harbouring a plasmid expressing FLAG-tagged EnrR in ChIP assays with a strain expressing FLAG alone as a negative control. EnrR-FLAG behaved similarly to wt EnrR because T3/T6SS production in the Δ*enrR* strain was fully restored by introducing the vector expressing EnrR-FLAG (Supplementary Figure S2D and S2F), thus validating the subsequent ChIP-associated analysis. Two independent ChIP-seq analyses with a FLAG-specific monoclonal antibody enabled exploration of the EnrR-binding landscape in the *E. piscicida* genome. In total, we identified 160 enriched loci harbouring EnrR-binding peaks (enriched by ≥2.0-fold compared with the control sample) (Supplementary Table S3) located across the genome, including the intergenic (58%) and coding regions (42%) of the genes (Figure 5A). These peaks were not present in ChIP-seq datasets from experiments in the control strain expressing FLAG alone (Figure 5A). Subsequent ChIP–qPCR analyses with *E. piscicida* strains chromosomally expressing FLAG-tagged EnrR (WT::P_{enrR}-EnrR-FLAG) or FLAG alone (Δ*enrR*::P_{enrR}-FLAG) at the native *enrR* locus validated that all 160 ChIP-seq-identified loci were *bona fide* EnrR-binding targets (Supplementary Table S3). In particular, an EnrR-binding peak could be found flanking the *esrB* gene (fold change = 2.0). Additionally, other obvious peaks were observed to localize to the promoter regions as well as intragenic regions of T3/T6SS gene clusters. These included peaks upstream of the major promoters of *evpP* (enriched by 2.8-fold), *esaR* (2.0) and *esrC* (1.5) (Figure 5A) (22). The recruitment of EnrR to these promoters also facilitates T3/T6SS gene expression, as combined deletion of *esrB* or *esrC* with *enrR* led to a much more severe decrease in T3/T6SS-related transcripts (Supplementary Figure S2G).

A survey of the ten top scoring peaks (Supplementary Table S3) highlighted the major EnrR-binding gene targets (Figure 5A). The top two binding peaks occurred upstream of its own gene (enriched by 4.2-fold) and the gene ETAE_2212 (*ybjD*) (4.2), encoding ATP-dependent endonuclease of the OLD family, implying autogenous control and possible roles in the prophage lysogenizing system (46). The third highest scoring site overlaps the promoter region of *torT* (3.9), encoding the periplasmic sensory protein associated with the TorRS two-component system. Of the top hits, the fourth and eight encode *galF* (3.9) and *agaW* (3.8) in the phosphotransferase system (PTS), respectively. The fifth peak is located between the intergenic region of a putative gene involved in a chromosome partitioning protein (ETAE_3427) and a putative integrase encoding gene (ETAE_3428). The sixth top peak is located at genomic islands (GI20) encoding a putative invasion containing featured LysM and Big domains (47). The ninth and tenth highest scoring sites are attributed to *mcp* involved in chemotaxis and a gene putatively encoding a multidrug efflux pump, respectively. Collectively, these data suggest that EnrR may be involved in various processes. The

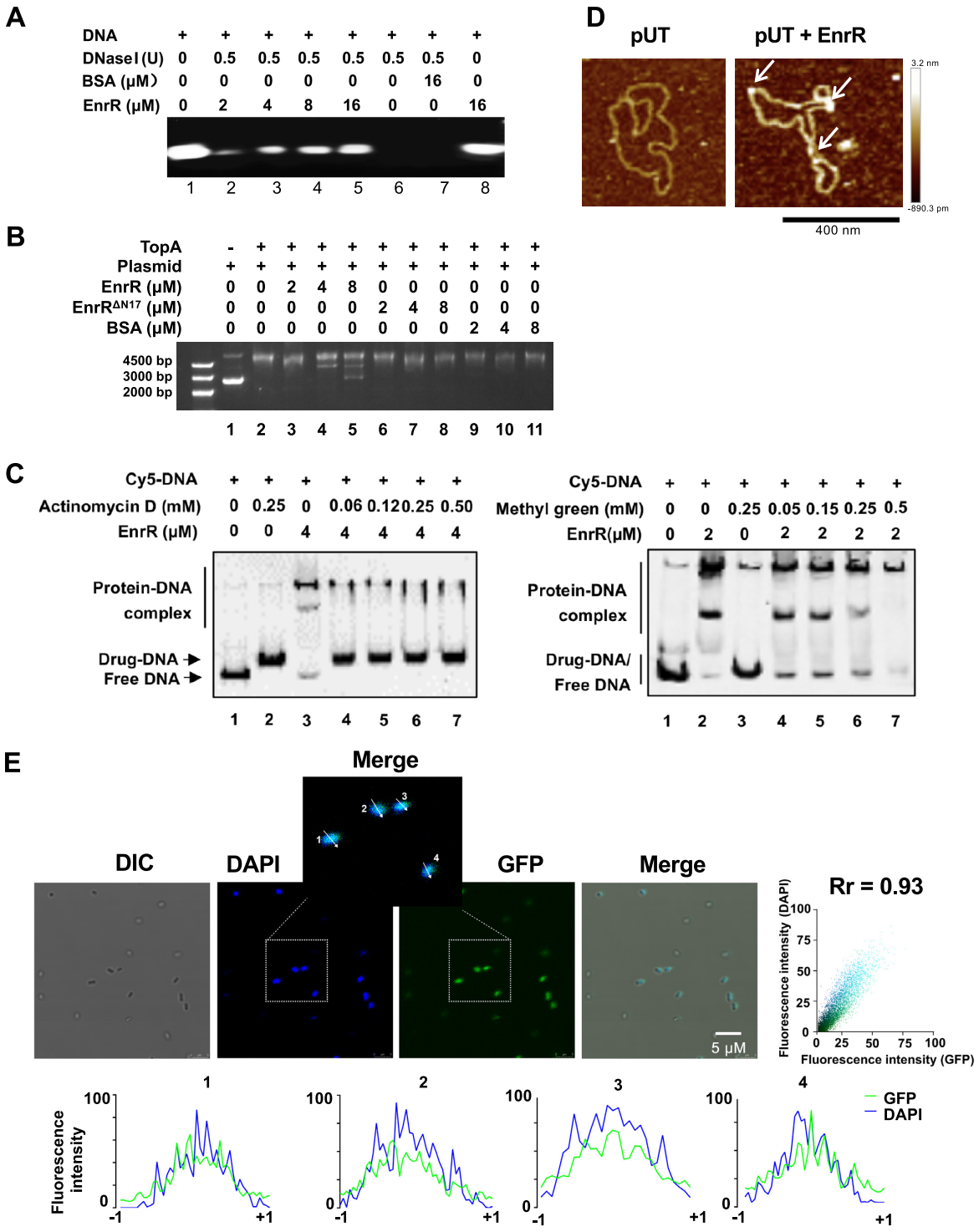

Figure 4. Identification of EnrR as a novel NAP. (**A**) DNase I protection ability assay of EnrR. DNA was incubated with different concentrations of EnrR and then digested with 0 or 0.5 U of DNase I for 5 min. The recovered DNA was run on an agarose gel. BSA was used as a control. (**B**) EnrR altered the plasmid supercoiling conformation. Plasmid DNA was incubated with different concentrations of EnrR or EnrR$^{\Delta N17}$, an EnrR variant with truncation of the N-terminal 17 residues (to be described later), in the absence or presence of topoisomerase A (TopA). BSA was used as a control. The recovered plasmid was analysed on an agarose gel. (**C**) EnrR binds to the DNA minor and major grooves. Cy5-labelled P_{esrB} fragments (10 and 40 ng for actinomycin D and methyl green competition assays, respectively) were incubated with EnrR protein in the presence of methyl green and actinomycin D. (**D**) AFM imaging assay for the protein–DNA complexes formed by EnrR and DNA. Images of circular plasmid DNA (5 ng/μl pUT) with or without 1 μM EnrR were acquired. (**E**) Colocalization assays for GFP-tagged EnrR with the bacterial nucleoid. The *E. piscicida* strain chromosomally expressing GFP-tagged EnrR in the native *enrR* locus was incubated on LBA with DAPI for 30 min. Images were acquired under 288 and 405 nm excitation. GFP (green) and DAPI fluorescence (blue) profiles are shown with the relative fluorescence intensity (*y*-axis) and cell positions, with -1 and + 1 indicating the fluorescence area (*x*-axis). Pearson's correlation coefficient (*R*r) between DAPI and GFP localization is also shown.

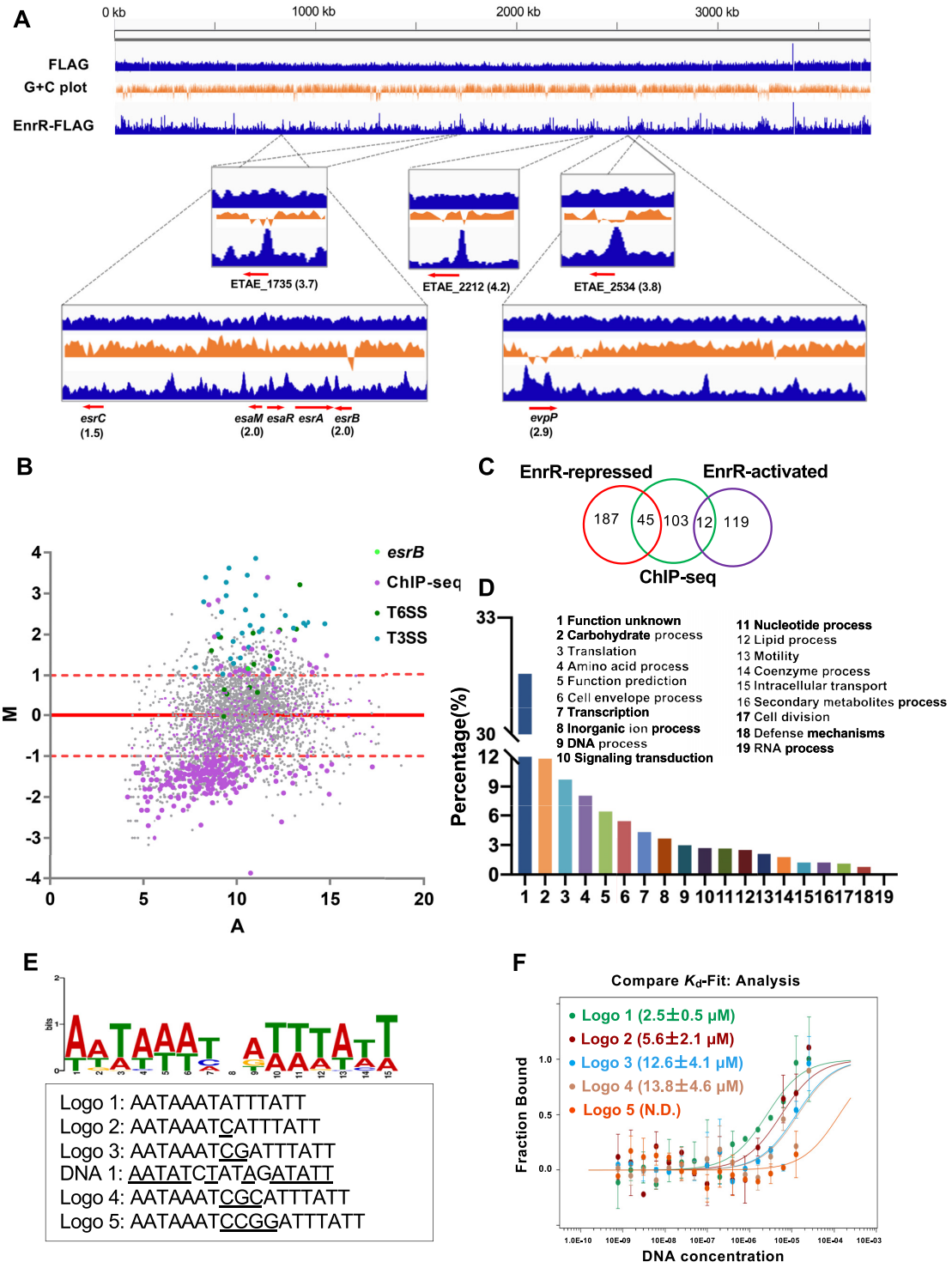

Figure 5. Genome-wide mapping of EnrR binding and verification of the binding site. (**A**) MACS view of EnrR binding across the *E. piscicida* genome as determined by ChIP-seq. The peak height (*y*-axis) indicates the sequencing read depth at each genomic position (*x*-axis). The inset boxes show significant EnrR binding sites identified over the indicated genes and T3/T6SS loci. The fold enrichment of binding sites around the promoter region of the indicated genes is shown in brackets by comparison of the strain expressing FLAG-tagged EnrR and with that of the FLAG tag alone. The genomic G + C plot is shown in red (window size of 1000 bp for overview or 200 bp for indicated genes). (**B** and **C**) MA-plot illustration (B) of the differentially expressed genes in wt and Δ*enrR* cells grown in DMEM, and the Venn diagram (C) showing genes directly bound and regulated by EnrR as revealed by RNA-seq and ChIP-seq analysis. The $\log_2$ of the ratio of the abundances of each transcript between the two conditions (M) is plotted against the average $\log_2$ of the abundance of that transcript in both conditions (A). T3/T6SS genes and ChIP-seq-enriched genes are highlighted (B). (**D**) Functional categories of the EnrR-regulated genes identified by RNA-seq and ChIP-seq. (**E**) EnrR-binding motif (Logo 1) derived from MEME analysis of the ChIP-seq peaks as well as the respective mutants are shown. (**F**) MST analysis of EnrR binding to the ChIP-seq consensus probe (Logo 1) and derived mutants (Logo 2–5) (E). Purified EnrR protein labelled with RED-tris-NTA dye was incubated with diluted DNA probes in MST assays ($n = 3$).

direct binding of EnrR to these loci—e.g. P_{esrB}, P_{2122} and P_{evpP}—was further validated using EMSA (Supplementary Figure S4A). Additionally, EnrR seems to bind to fragments of $P_{2122}$with various sizes and/or G + C contents (Supplementary Figure S4B). Furthermore, the B1H assays, DNase I footprinting and MST further proved the interaction of EnrR with these DNA molecules *in vivo* and *in vitro* (Supplementary Figure S4C-E) (47).

Transcriptomics analysis of the wt and Δ*enrR* strains grown in DMEM indicated that 363 genes were regulated ($|\log_2 FC| \geq 1$-fold, $P_{adj} < 0.05$) (Figure 5B) (Supplementary Table S4), of which 232 genes were upregulated and 131 genes were downregulated in Δ*enrR* compared with wt (Figure 5B and C). Although the expression of most (103/160) genes highlighted by ChIP-seq was not affected in the Δ*enrR* strain, T3/T6SS-associated genes were included in the list of genes most prominently regulated by EnrR (Figure 5B) (Supplementary Table S4). COG analysis showed that 31% of the genes controlled by EnrR are hypothetical or have unknown functions (Figure 5D). These results suggest that EnrR is a global regulator that binds to various genes and modulates their expression.

EnrR targets DNA regions harbouring AT-rich consensus sequences

Analysis using the MEME (multiple EM for motif elicitation) algorithm revealed a palindromic consensus (5′-AATAAATNATTTATT-3′) ($E < 0.05$) in the EnrR-binding sequences revealed by ChIP-seq (Figure 5E). This consensus DNA (Logo 1) showed high affinity for EnrR, and the K_d value for their interaction was assessed as 2.5 ± 0.5 nM by MST analysis (Figure 5F). The EnrR-DNA binding affinity decreased with increasing spacer N length ($N = C/G$; Logo 2 - Logo 5 designed based on Logo 1), and when its length reached the 4-mer, the binding affinity was barely detected (Figure 5F). These analyses suggested that EnrR targeted DNA fragments with AT-rich consensus.

The overlapping ChIP-seq- and RNA-seq-enriched regions/genes were broadly distributed on the low G + C content regions corresponding to all GIs. Although GI7 (T3SS) and GI17 (T6SS) displayed overall higher G + C contents (62.5% and 64.6%, respectively) than the genome average of 59.7% (16), there was also consistency in EnrR recruitment and a lower G + C content in the ChIP-seq-identified regions, including the *evpP* promoter region (Figures 5A and 6A). qRT-PCR analysis validated that the transcription levels of selected genes at GI6, GI11 and GI16 were all significantly higher in the Δ*enrR* strain than in the wt strain and were reduced to that of the wt level in the Δ*enrR*/P_{0456}-*hns* strain overexpressing H-NS (Figure 6B). Consistent with this result, we commonly observed that the cultures of *E. coli* BL21 harbouring the EnrR expression plasmid pET-*enrR* became transparent and that bacterial growth could be largely restored by coexpressing H-NS (Supplementary Figure S6A). Bacterial lysis and cell wall disruption were observed for the cells expressing EnrR (Supplementary Figure S6B). Following extrachromosomal DNA extraction and phage enrichment from the supernatants of EnrR-expressing *E. coli*, phage Mu D108-like DNA and the corresponding phage particles were isolated (Supplementary Figure S6C,D) followed by DNA sequencing confirmation.

Additionally, statistical analysis of the ChIP-enriched DNA sequence verified that EnrR was more intensively recruited to higher A + T content regions, including the GI regions, than to other regions (Figure 6C). Similar to other NAPs for Gram-negative bacteria (3–5), a positive correlation between AT% and the protein recruitment level was also found for EnrR (Figure 6D; Pearson's rho = 0.93; $P < 0.001$ compared with ORFs). We further characterized the potential relationship between the oligonucleotide composition of the ChIP-seq peaks (tetranucleotide, trinucleotide and dinucleotide) and EnrR recruitment levels. TpA dinucleotides (TpA steps), among all dinucleotide steps in AT-rich DNA, confer the most flexibility on DNA by facilitating the accommodation of DNA-interacting residues of DNA binding proteins—e.g. xenogeneic silencers—in the minor groove (3,48). EnrR-enriched sequences harbouring the TpA step and trinucleotides containing TpA had the highest (Spearman's rho = 0.137; $P = 0.00042$) positive correlation with the EnrR recruitment level (Figure 6E). Taken together, these results suggest that EnrR is a global regulator prone to target and inhibit the expression of horizontally acquired foreign AT-rich genes.

Structural basis for target DNA binding by EnrR

EnrR shares approximately 45% sequence identity with the NER protein of phage Mu, whereas the sequence similarities between EnrR and other DNA-binding phage proteins, including cro and λ repressor proteins, are low (Figure 7A). To unravel the underlying mechanism of DNA binding by EnrR, we performed crystallographic studies and solved the EnrR-DNA complex structure at high resolution (Table 1). Initial trials of crystallization with EnrR and the 14-mer Logo 1 derived from the MEME analysis of the ChIP-seq data (Figure 5E), and many other putative oligos failed because of low diffraction qualities. We used one self-complementary DNA (DNA1: 5′-CGAAATATCTATAGATATTTCG-3′, the underlined base identical or close to Logo 1) in the crystallization trials. This AT-rich DNA oligo contains the modified Logo 1 DNA sequence and extra CGA in the 5′ upstream region and appears not to be involved in EnrR-DNA binding but may facilitate the stability of the DNA–protein complex with CG pairs. In the complex structure, each DNA1 duplex interacts with two EnrR molecules (Figure 7B). The overall folding of the two EnrR molecules is almost identical, as indicated by the very low root mean square deviation value (rmsd, 0.16 Å). EnrR contains four α-helices (α1- α4, Supplementary Figure S7A), and its surface is highly positive in charge (Supplementary Figure S7B).

EnrR binds at the major groove (Figure 7B and Supplementary Figure S7C), forming extensive interactions with the phosphate backbone of the DNA1 duplex (Figure 7C). A5 of DNA1 forms two hydrogen-bond (H-bond) interactions with the side chain of Arg40 (Figure 7D). T6 of DNA1 forms three H-bonds, including one with the side chain of

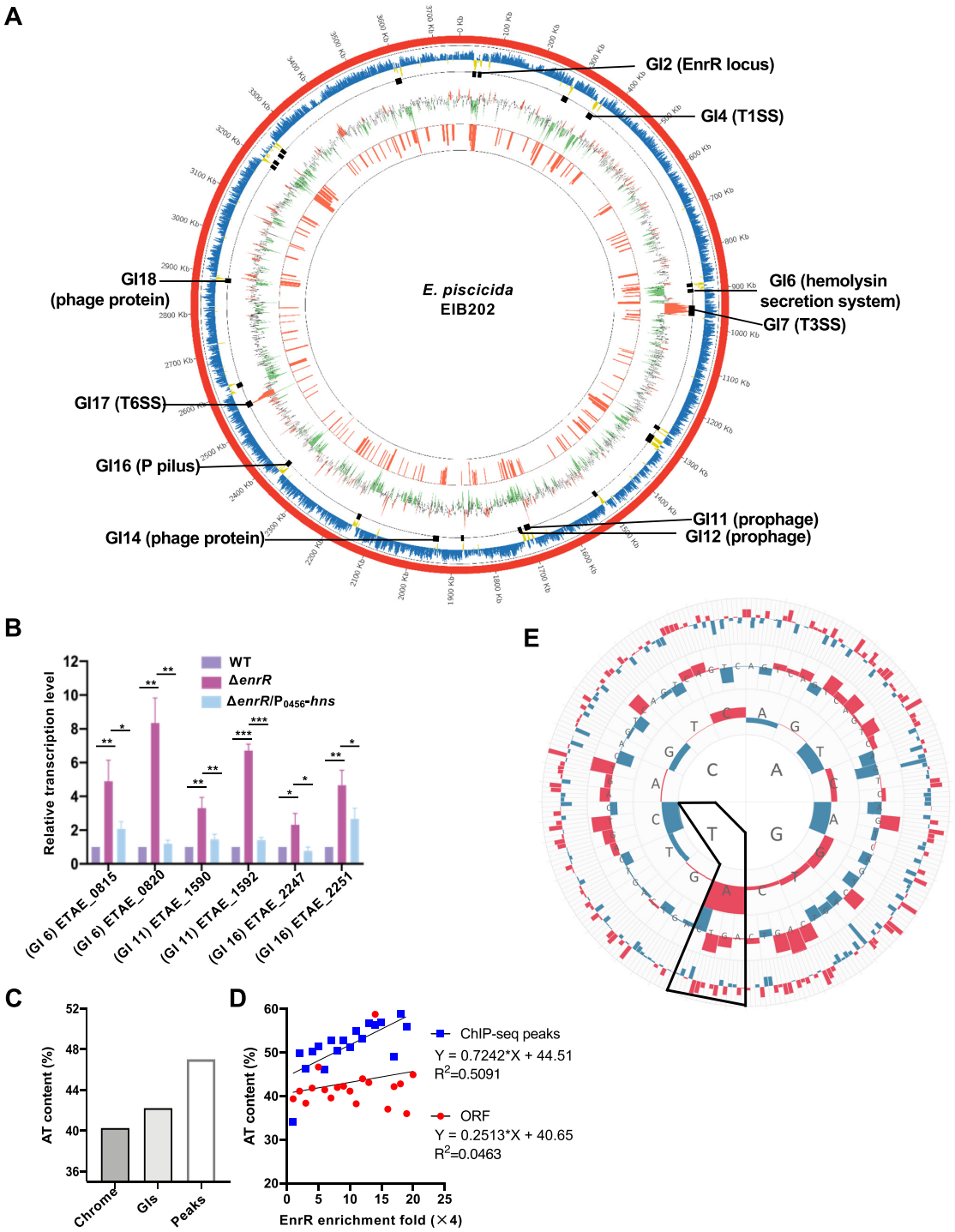

Figure 6. EnrR targets AT-rich GIs and gene regions across the chromosome. (**A**) Circular genomic map of the G + C content (circle 1 from outer circle; above or equal to the median G + C content (blue), less than the median (yellow)), RNA-seq (circle 2; orange indicating EnrR-activated genes and green depicting EnrR-repressed loci) and ChIP-seq (circle 3; the enriched binding sites). The annotated genomic islands (GIs) are shown. (**B**) Transcript levels of the annotated GI genes in wt-, Δ*enrR*-, and Δ*enrR*-overexpressing H-NS (Δ*enrR*/P_{0456}-*enrR*) cells grown in LB medium for 12 h. *gyrB* was used as the internal control. The results shown are means ± S.D. ($n = 3$). ***, $P < 0.001$; **, $P < 0.01$ and *, $P < 0.05$ compared with wt based on Student's *t*-test. (**C**) AT% content of ChIP-seq peak-associated genes (peaks) compared with the averages of GIs and the chromosome (Chrome). (**D**) Relationship between averaged AT% values (*y*-axis) of pooled ChIP-seq peaks (with 100 bp central region; blue square) or the corresponding ORFs (red circle) and mean EnrR enrichment folds (*x*-axis) determined in the ChIP-seq analysis. The dataset of the EnrR enrichment fold was scaled by 4 and divided into 20 ranges to pool the corresponding ChIP-seq peaks and ORF sequences in each of the regions. (**E**) The height of the red/blue bars represents the positive/negative coefficient (Spearman's rho) between the oligonucleotide usage deviations and EnrR recruitment levels in ChIP-seq peaks. Bar scales: −0.171∼0.137 (dinucleotide), −0.167∼0.160 (trinucleotide), −0.299∼0.218 (tetranucleotide). Oligonucleotide compositions of the 100 bp central regions of ChIP-seq peaks were analyzed.

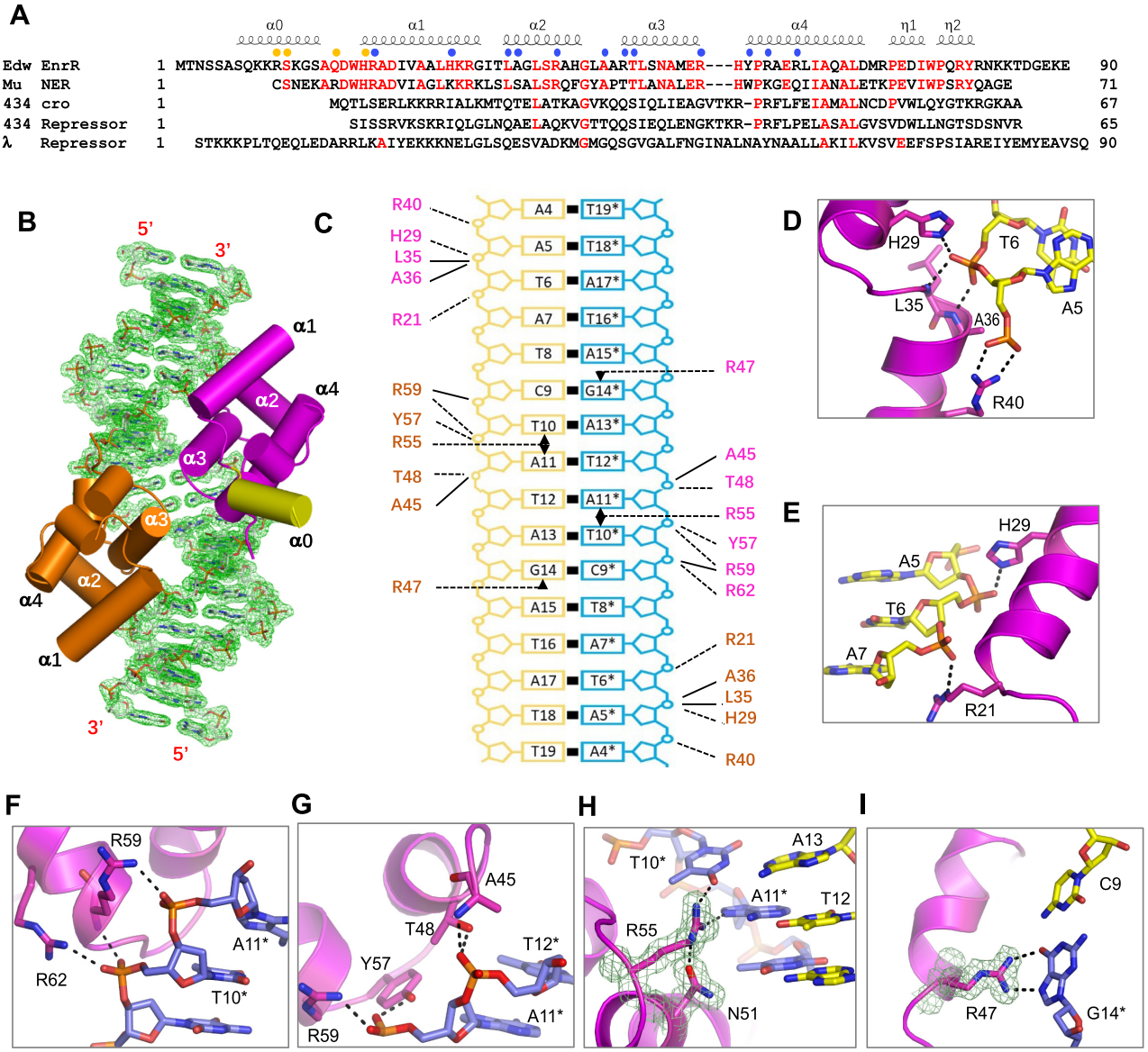

Figure 7. Crystal structure of the EnrR-DNA1 complex. (**A**) Sequence alignment of EnrR from *Edwardsiella piscicida* (Edw) using HTH motif-containing proteins from various phages. (**B**) Overall structure of the EnrR-DNA1 complex. The two EnrR molecules are shown as cartoons in brown and magenta and yellow, respectively. The DNA1 duplex is shown as sticks outlined with 2Fo-Fc electron density maps (contoured at the 1.5 sigma level). (**C**) Detailed interactions between DNA1 and the HTH motifs of EnrR. H-bond interactions mediated by the EnrR main chain and side chain atoms are indicated by dashed and solid lines, respectively. Nucleobase-specific recognitions are indicated by triangles. (**D–I**) Detailed interactions between the EnrR HTH motif and DNA.

His29 and two with the main chains of Leu35 and Ala36, which are located at the N-terminus of α2. A7 of DNA1 forms one H-bond with the side chain of Arg21 (Figure 7E). Arg21 and His29 reside at the N- and C- termini of α1, respectively. T10* and A11* of the complementary strand interact with the side chains of Tyr57, Arg59 and Arg62 of α4 (Figures 7F,G). Similar to other nucleotides, T12* also forms H-bond interactions with EnrR. However, instead of positively charged residues, T12* interacts with neutral residues Ala45 and Thr48 of α3 (Figure 7G).

In addition to the phosphate backbone, EnrR also recognizes the nucleobases T10* and A11*. The nucleobases of both T10* and A11* form H-bonds that interact with Arg55 (Figure 7H). The distance between the O4 atom of T10* and side chain NH1 atom of Arg55 is 2.8 Å, and the distance is 3.1 Å between the NH2 atom of Arg55 and the N7 atom of A11*. The conformation of Arg55 is further stabilized by its H-bond (2.6 Å) interaction with Asn51. Similar to T10* and A11*, the nucleobase of G14* also interacts with one Arg residue, Arg47, which is inserted into the DNA1 major groove. G14* and Arg47 form two H-bonds, one (2.7 Å) between the G14* O6 atom and Arg47 NH2 atom and the other (2.9 Å) between the G14* N7 atom and Arg55 NH1 atom (Figure 7I).

EnrR mediates conformational changes during DNA interaction

The crystal structures of the repressor of phage λ and cro and the repressor of phage 434 were reported previously (49). EnrR and these phage proteins all contain one HTH motif. However, possibly because of their low sequence similarities (Figure 7A), the overall folding of EnrR is significantly different from that of these proteins (Supplementary Figure S7D), a result supported by the high rmsd values (∼4.0 Å). EnrR is a monomer (Supplementary Figure S2I,J), and cross contacts between other monomers are mediated by Glu54, Arg55, and His56 (Supplementary Figure S8A). Through their side chains, Glu54 of one EnrR and Arg55 of the partner protein form direct H-bond interactions. Mediated by water molecules, Glu54 also forms extensive H-bond interactions with His56 of the partner protein. His56 is the only residue connecting the α3 and α4 helices. The lengths of the α3-α4 connecting loops are similar for EnrR and phage Mu NER protein, whereas they are significantly shorter than other HTH motif-containing proteins (Figure 7A). Perhaps because of the smaller size and tight contact of the α3-α4 loops, the two EnrR molecules pack closely to each other and recognize one potential consensus sequence of 5′-CTATAG-3′ (Figure 7C). Unlike the consensus sequences of the phage λ repressor and phage 434 cro and repressor, which are all very long and contain stretches of nonspecific nucleotides in the middle, the consensus sequence of EnrR is short and continuous.

We found that the DNA1 duplex was severely distorted following EnrR binding. The width of the DNA1 major groove is 22.9 Å at the central cross contact region of EnrR, which is wider than that of the regular B-form DNA duplex (17.6 Å) (Supplementary Figure S8B). Away from the central region, the DNA1 major groove was narrowed and only measured 15.3 Å at the boundary region of EnrR, which is 2.3 Å narrower than that of the regular B-form duplex (Supplementary Figure S8C). In addition to the DNA complex, we also solved one apo-structure of EnrR (Table 1). Although the overall folding of EnrR is similar in the apo- and complex structures, structural superposition could reveal some subtle conformational changes in EnrR (Supplementary Figure S8D). Following DNA binding, the N-terminus of EnrR α3 tilts slightly towards α2, perhaps because of the interaction between Arg47 and the nucleobase of G14* (Figure 7I). One apo NMR structure of phage Mu NER has also been reported (1NER). As revealed by structural superposition (Supplementary Figure S8E), the overall folding of NER is very similar to that of EnrR. Many DNA-interacting residues are conserved in EnrR and NER, indicating that the latter may follow a similar manner in target DNA binding.

The EnrR N-terminus promotes DNA binding and H-NS competition

EnrR is longer than phage Mu NER at the N-terminus for 10 aa residues. The N-terminus of EnrR is also longer than that of cro and the repressor of phage 434 by 16 and 18 aa, respectively (Figure 7A). In the apo-structure, the N-termini of all EnrR molecules are disordered. In the complex structure, the N-terminus of one EnrR molecule is disordered, but it folds into one short helix, α0 (aa 7–16), at the second molecule (Supplementary Figure S7A). α0 does not interact with the DNA1 duplex, but it inserts into the minor groove of the symmetry-related duplex, forming two direct H-bond interactions (Figures 8A–C). As depicted in Figure 8D, one H-bond is formed between the Arg11 NH1 atom and backbone OP1 atom of T8; the other H-bond is formed between the Ser12 OG atom and OP1 atom of C9. Gln17 resides at the α0–α1 linker region; its side chain forms one H-bond interaction with the nucleobase of C9 (Figure 8E). His20, the first residue of α1, also interacts with the backbone phosphate of the symmetry-related duplex (Figure 8F).

Similar to many NAPs (11), EnrR prefers to bind AT-rich DNAs, as confirmed by our abovementioned analyses (Figures 5E,F and 6) and structural data (Figure 7C). Altering the conformation of the target DNA is one common mechanism in regulating gene transcription by NAPs. However, different NAPs may use different strategies to change gene conformation (50–51). In the crystal lattice of the EnrR complex structure, many DNA1 molecules stack on each other, forming a continuous pseudoduplex (Figure 8C). Via their HTH motifs, many cross-contacted EnrR bind the pseudoduplex at the major groove. Next, the N-terminus of EnrR molecules binds to the minor groove of the nearby DNA duplex, leading to the aggregation and/or putative bending of the DNA. Such DNA binding and bending mechanisms are unique for EnrR and have not been documented for other NAPs.

To verify the DNA binding mechanisms observed in the EnrR-DNA1 complex, we characterized several EnrR variants with single-point mutations or deletion of N-terminal residues 1–17 (ΔN17) corresponding to the α0 domain. As illustrated in Figure 8G, the Δ*enrR* mutant strains expressing wt or mutant forms of EnrR, EnrR^{Q17G}, EnrR^{R47G}, EnrR^{Q55G}, EnrR^{H17G} and EnrR$^{\Delta N17}$ showed various levels of T3/T6SS production. The significantly decreased EseB/C/D and EvpC yields in the strains expressing R47G and R55G variants of EnrR and their abolished or markedly decreased DNA-binding capacities further demonstrated their essential roles in the HTH domain-mediated EnrR–DNA interaction (Figures 7H,I and 8G,H). Additionally, the mutants producing EnrR^{Q17G} and EnrR$^{\Delta N17}$ generated markedly lower levels of T3/T6SS proteins (Figure 8G), a finding that agrees with the drastically impaired DNA binding in EnrR^{Q17G} (Figure 8H) and EnrR$^{\Delta N17}$ (Supplementary Figures S5F, S9A and S9C). Similarly, EnrR$^{\Delta N17}$ showed no resistance to the DNA relaxation activity of TopA (Figure 4B) and exhibited a deficiency in DNA oligomerization (Supplementary Figure S5F) compared with wt EnrR. Importantly, EnrR$^{\Delta N17}$ could no longer compete with H-NS in P_{esrB} DNA binding (Figure 8I). Collectively, these analyses demonstrated that the unique DNA binding mediated by the N-terminal α0 domain is essential for EnrR to antagonize H-NS and facilitate bacterial virulence gene expression.

DISCUSSION

In the present study, analysis of an *in vivo* TIS dataset with the PACE algorithm (19) allowed identification of a new

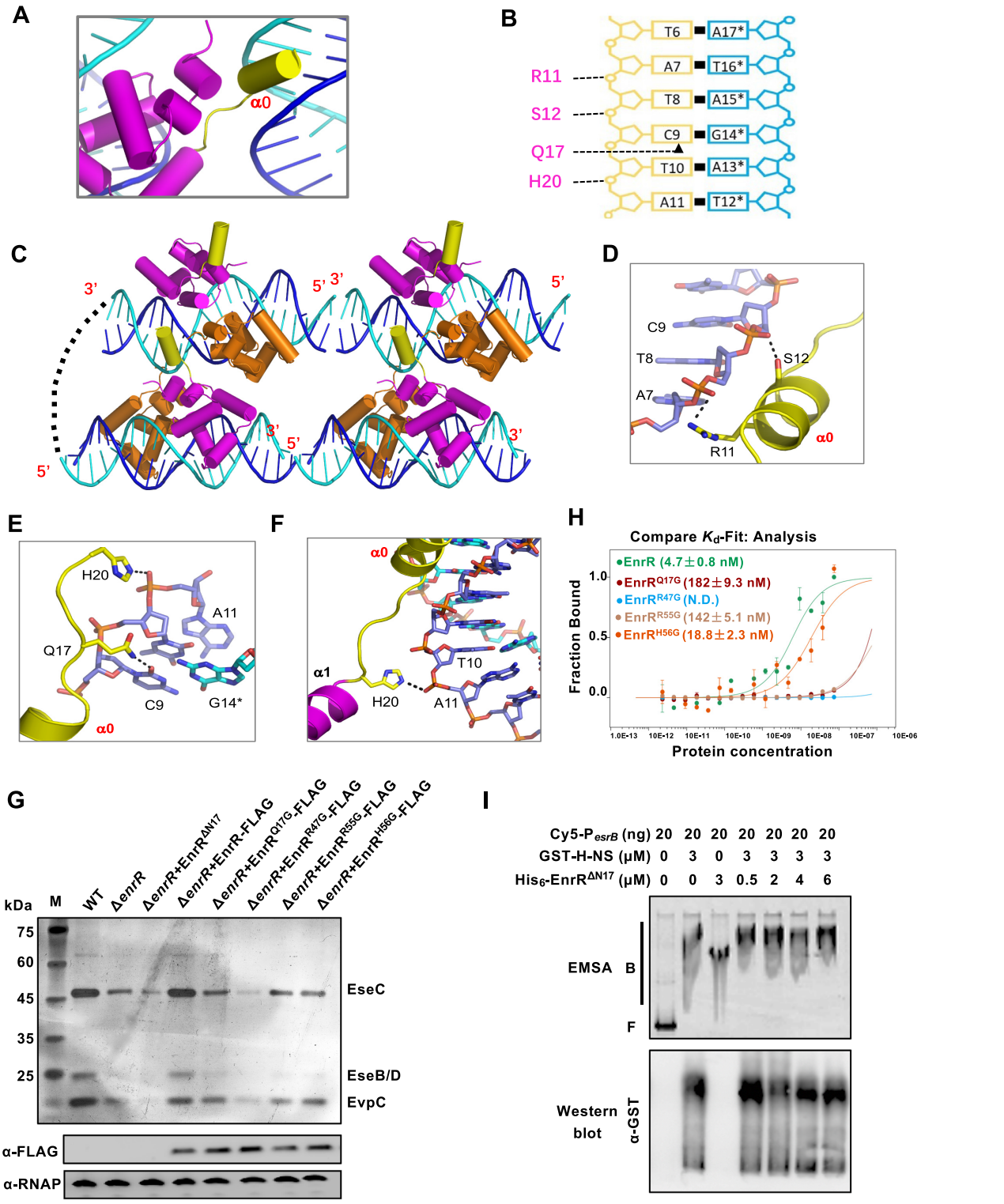

Figure 8. N-terminal α0 facilitates the EnrR interaction with the DNA duplex and competition against H-NS. (**A** and **B**) Interactions between EnrR α0 and the symmetry-related DNA duplex. (**C**) Packing and interactions of EnrR and the DNA1 duplex in the crystal lattice of the complex structure. (**D–F**) Detailed interactions between EnrR α0 and the symmetry-related DNA1 duplex. (**G**) Production of T3/T6SS proteins in the wt, Δ*enrR* or Δ*enrR* strain expressing FLAG-tagged wt or variant EnrR (Q17G, R47G, R55G, H56G and ΔN17 (deletion of N-terminal 17 residues)) based on the pUT plasmid. The SDS–PAGE resolved proteins were blotted with anti-FLAG specific antiserum (lower panels). RNAP was used as the loading control for the blots. (**H**) Cy5-P$_{esrB}$ DNA binding capacities of the wt and EnrR variants analysed by MST. The assays were performed in triplicate and are shown as means ± S.D. (**I**) The N-terminal α0 domain is essential for EnrR competition with H-NS in P$_{esrB}$ DNA binding. The top panel shows EMSA containing Cy5-labelled P$_{esrB}$ DNA and either purified GST-tagged H-NS or EnrR^{ΔN17}. In the bottom panel, the EMSA gels were transferred to a PVDF membrane and probed for H-NS using anti-GST antibodies.

virulence regulator, EnrR, in *E. piscicida*. EnrR is encoded in GI2 and is possibly horizontally acquired (16). We revealed that EnrR derepresses *esrB* expression by competing with H-NS binding to facilitate T3/T6SS production and *in vivo* virulence in *E. piscicida*. The introduction of the *enrR* gene in *E. anguillarum* or *S. tyhpimurium* strains strongly augments their virulence gene expression. EnrR functions as a novel NAP that colocalizes with the bacterial nucleoid. Global profiling of EnrR-DNA binding and gene regulation of various processes indicated that the protein targets AT-rich genomic regions or GIs and represses their expression. Structural analysis confirmed EnrR binding to DNA containing the TA-rich palindrome and illuminated its unique DNA binding ability to both major and minor grooves. Collectively, we show that EnrR is a unique NAP that plays roles as an H-NS-antagonizing virulence activator targeting AT-rich DNA. Thus, our findings suggest that bacterial pathogens have evolved exquisite mechanisms to acquire and manage xenogeneic NAPs to interact with endogenous NAPs and MGEs to balance virulence adaptation and regulatory integrity.

Similar to analogues in *Salmonella* and other bacterial pathogens, *Edwardsiella* T3/T6SS gene clusters are crucial GIs horizontally acquired as MGEs and subjected to sophisticated regulation during various growth conditions. Usually, their expression is repressed by factors—e.g. RpoS—under *in vitro* conditions and during the initial stages of the *in vivo* infection process (25,52). Previous investigation and evidence from this study also showed that the major xenogeneic silencer H-NS inhibited T3/T6SS production because of its binding to the *esrB* promoter region and putative binding to other loci on these two GIs (Figure 3) (27–28). The local- and long-distance *cis*-effects of these H-NS binding or nucleation sites on the promoter activities of *esrB* and other T3/T6SS promoters—e.g. *esrA*, *esrC*, *esaR*, *esaM*, *evpA* and *evpP*—warrant further characterization. However, the bacterium must overcome these repression mechanisms to activate T3/T6SS expression for *in vivo* systemic infections or under other conditions requiring these secretion systems for survival. Here, we revealed that *E. pisicicida* has evolved a mechanism to leverage putatively horizontally acquired EnrR to abrogate H-NS-mediated silencing and activate the *esrB* promoter and T3/T6SS production.

Currently, *Edwardsiella* bacteria comprises five species, the T3/T6SS-containing species *E. ictaluri* and *E. piscicida*, *E. anguillarum* and the non-T3/T6SS lineages of *E. hoshinae* and *E. tarda* (15). Thus, *Edwardsiella* is analogous to *Salmonella* (14,53), the model genus to study GI evolution and regulation. *E. ictaluri* and *E. piscicida* encode only one set of T3SS and T6SS genes, while *E. anguillrum* harbours additional sets of T3/T6SS clusters. Additionally, *E. anguillrum* showed lower DDH/ANI similarities to *E. tarda* than those of *E. ictalurid*/*E. piscicida* to *E. tarda*, suggesting that *E. anguillarum* appeared later than *E. piscicida* (15). Because *E. anguillarum* strains do not encode EnrR, we showed that ectopic expression of EnrR in *E. anguillarum* could augment T3/T6SS yields (Figure 2F,G), further explaining their differences in pathogenesis and virulence gene evolution. Evolutionary scenarios could be proposed that after acquiring T3/T6SS genes, the ancestral *Edwardsiella* bacteria (representing the EdwGI lineage) (17) could evolve into EdwGII, including *E. anguillarum*, by the accompanying acquisition of EsrAB, or into *E. piscicida* by acquiring additional EnrR to allow a higher capacity for T3/T6SS expression by antagonizing H-NS repression (Figure 9A–D). Some strains of notorious enteric pathogens—e.g. *S. enterica*, *E. coli* and *Yersinia enterocolitica*—also encode EnrR homologues (Supplementary Figure S1); similar virulence evolution events involved in these proteins might exist.

Here, using RNA-seq and ChIP-seq, we defined the EnrR control of gene expression in *E. piscicida* (Figure 9E). Among the 131 EnrR-upregulated genes, T3/T6SS genes ranked at the top of the list. EnrR also positively controls the PhoP/PhoQ two-component system, which is involved in global gene expression (54). Lipid transport and metabolism, F_0F_1-type ATPase, and lysogeny/lytic switch systems are also under direct or indirect control by EnrR (Supplementary Tables S3 and S4). However, EnrR negatively regulates ∼232 genes classified into several key processes, including flagellar biosynthesis, pilus assembly, biofilm formation, chemotaxis, antibiotic resistance and DNA recombinase, which have been established as MGE genes (Supplementary Tables S3 and S4). Many of these genes are located in GIs and may be essentially involved in the pathogenesis of the bacterium. The promoters of genes associated with all 24 GIs recruit EnrR and are under direct control by the protein (Figure 6A). Additionally, the core genes related to metabolic processes, including the sugar phosphotransferase system (PTS) and acetyl-CoA acetyltransferase, and those linked to cell division and cell wall biosynthesis, were also subject to EnrR regulation (Figure 5D). Furthermore, EnrR can regulate the lysogeny/lytic lifestyle of the prophages in *E. coli* (Supplementary Figure S6) and enhance virulence in *S. Typhimurium* SL1344 by activating SPI-2 expression (Supplementary Figure S3). These analyses feature EnrR as a master regulator and an NAP globally controlling gene expression (Figures 6A and 9E).

It is intriguing to examine the underlying mechanisms by which EnrR counteracts H-NS silencing on the *esrB* promoter. Bacterial pathogens deploy many counter silencers, the factors that counteract H-NS or other xenogeneic silencers on foreign gene expression for dynamic regulation of virulence gene expression during *in vivo* infection or *in vitro* growth. *Salmonella* employs countersilencers, including SsrB (32,45), PhoP (53), LeuO (55), CsgD (56) and SlyA (57), to counteract H-NS-mediated repression of virulence gene expression in response to various signals. Currently, we cannot exclude EsrB and other countersilencers that may be used to antagonize the H-NS repression of *esrB* and other promoters associated with T3/T6SS in an EnrR-dependent manner in *Edwardsiella* bacteria. The intrinsic promoter architecture of *esrB* is unique because it contains several binding sites for EnrR and H-NS and accommodates multiple EnrR/H-NS molecules (Figure 3C). Additionally, the binding sites of EnrR and H-NS appear not to overlap (Figure 3C–E) and may require EnrR's N-terminal extension mediated minor groove contacts and cooperative DNA binding in the far apart DNA duplex to form DNA loop and compaction for its occlusion of H-NS binding to DNA minor grooves (Figure 3F–G). Thus, *esrB* could be derepressed under physiologically permissive conditions (14). Notably,

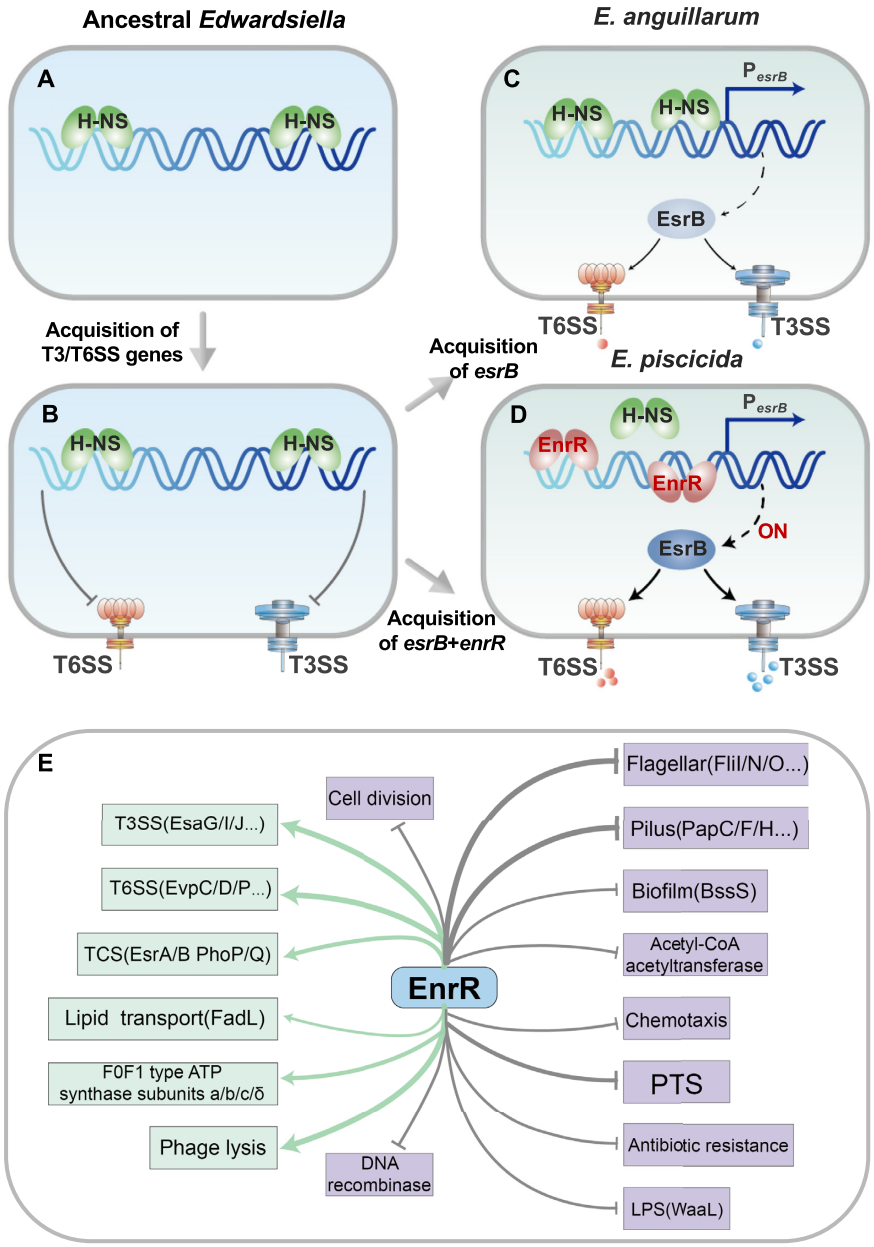

Figure 9. Model of horizontally acquired NAP EnrR interacting with endogenous H-NS to modulate the expression of T3/T6SS and other genes. (**A–D**) Along with *Edwardsiella* evolution, the ancestral strain expressing housekeeping H-NS (A) and then acquired T3/T6SS GIs (B), following obtaining of the genes for the two-component system EsrA-EsrB in *E. anguillarum* (**C**) and EsrA-EsrB and EnrR in *E. piscicida* (**D**). In *E. piscicida*, the acquisition of EnrR antagonizes H-NS repression, leading to high T3/T6SS production and pathogenicity toward hosts. (**E**) Summary of EnrR target genes and related expression profiles. Green and purple solid lines indicate activation and repression, respectively.

the ChIP-seq enriched peak mapped to the *esrA-esrB* intergenic region did not exactly match the neighbouring locus of the lowest G + C content in P_{esrB} (Figure 5A). We hypothesized that EnrR might mediate long-range interactions between these *cis*-elements, a claim that warrants future investigation. Alternatively, because EnrR appeared to bind the promoter region of *esrB* and augment its transcription in an H-NS-independent manner (Figure 3A, lanes 9–10), it could also play a role in transcriptional activation by direct recruitment of RNAP to P_{esrB}. How these NAPs or transcriptional regulators intertwine and coordinate to tightly control *esrB* transcription in a direct activation mode or silencing-anti-silencing manner as well as other genomic transactions, such as chromosome supercoiling (58–59), remains to be investigated.

Usually, H-NS silences gene expression by occluding and blocking RNAP transcription initiation of specific promoter regions from the ends of a stiffened nucleoprotein filament (60). Counter silencers such as PhoP (53), VirB (61) and SsrB (45) use disruptive countersilencing mechanisms to alter the DNA–protein complex structure to disrupt H-NS-mediated silencing, which directs the binding or pro-

cessing of RNAP. However, H-NS remains bound or condensed to a promoter region even under countersilencing conditions by these proteins (53,60). This finding is different from EnrR, which largely evicts H-NS from the promoter (Figure 3F). Given that EnrR does not interact with H-NS directly (Supplementary Figure S4F), we also hypothesized that EnrR might not prevent H-NS oligomerization to derepress gene expression similar to H-NST-like proteins (62–63), Ler (64) and LeuO (65). AFM also demonstrated that the DNA-binding and oligomerization modes of EnrR are different from those of Ler. Although EnrR forms large particles with DNA at high concentrations, it appears to wrap, stiffen and bridge DNA at lower concentrations (Figure 4D and Supplementary Figure S5A–E). Ler protein forms compact particles wrapped by contour-length shortened DNA (66). Additionally, the dynamic derepression mechanisms by which EnrR induces T3/T6SS in response to various cues during the infection state warrant future investigation. Collectively, these analyses suggested that EnrR might adopt a distinct mechanism to compete for H-NS binding to the *esrB* promoter and activate its transcription.

Xenogeneic silencers are a group of specific NAPs (67). To date, five families of xenogeneic silencers have been identified, such as H-NS, in numerous bacteria that selectively repress the expression of foreign sequences and contribute to bacterial genome evolution (48,68). Xenogeneic silencers share a domain architecture common with an N-terminal oligomerization domain and C-terminal DNA binding domain that facilitate cooperative binding to high- and low-affinity DNA sites and promote the formation of nucleation filaments, chromosome compaction and gene silencing (48,69). Although EnrR targets AT-rich DNA fragments, we hypothesized that EnrR, as a novel NAP, might not be classified as a typical xenogeneic silencer because of its apparent lack of an oligomerization domain (Figure 1C and 7A). Additionally, EnrR binds to both DNA major and minor grooves with its HTH domain and the N-terminal extension (α0) residues, respectively (Figure 7), in contrast to documented xenogeneic silencers that specifically bind to the minor grooves of DNA targets (48). The observed TpA steps in the EnrR target DNA (Figure 6E) explain its favoured binding to the minor grooves (48) by the N-terminal extension (α0) residues. Given the essential roles of the N-terminal helix (α0) in EnrR DNA binding (Figure 8I; Supplementary Figures S5F and S9C) and gene regulation and the observed tandem binding sites upstream of the *esrB* promoter region, this unique DNA binding mode might facilitate DNA looping, bridging or even compaction to organize GI regions or chromosomes in a higher-order hierarchy. Whether EnrR can cooperatively interact with or facilitate the cooperativity of xenogeneic silencers—e.g. H-NS—to bind and bridge DNA remains to be determined.

DATA AVAILABILITY

Accession numbers are available for the SRA data, PRJNA734738 and PRJNA767449 for RNA-seq and ChIP-seq, respectively, and the PDB structural data, 7F9I and 7F9H for apo-EnrR and EnrR-DNA complex, respectively.

SUPPLEMENTARY DATA

Supplementary Data are available at NAR Online.

ACKNOWLEDGEMENTS

We thank the staff of BL17U1 beamline at the Shanghai Synchrotron Radiation Facility (SSRF) and Large-scale Protein Preparation System at the National Facility for Protein Science in Shanghai (NFPS), Zhangjiang Lab, Shanghai Advanced Research Institute, CAS, for help during data collection. The authors also thank Dr. Jian Jiao (CAU) for his helpful discussions.
Author Contributions: Conceptualization: WQ; Data curation: W.Q., M.R., L.Y., G.J.; Formal analysis: Z.Y.X.; Investigation: M.R., L.Y., S.S., G.J., Q.H., M.J., Z.Y., B.Y.; Writing—original draft: M.R., L.Y., S.S., G.J.; Writing—review and editing: W.Q., S.S., Z.Y.X., M.R.

FUNDING

National Key Research and Development Program of China [2018YFD0900504 to Q.W.]; National Natural Science Foundation of China [32130108 to Q.W.]; Shanghai Municipal Science and Technology Commission of Shanghai Outstanding Technology Leaders plan [21XD1431900 to Q.W.]; Innovation Group Project of Southern Marine Science and Engineering Guangdong Laboratory (Zhuhai) [311020005 to Y.X.Z.]; China Agriculture Research System of MOF and MARA [CARS-47-17 to Q.W.].
Conflict of interest statement. None declared.

REFERENCES

1. Pallen,M. and Wren,B. (2007) Bacterial pathogenomics. *Nature*, **449**, 835–842.
2. Ross,B.D., Verster,A.J., Radey,M.C., Schmidtke,D.T., Pope,C.E., Hoffman,L.R., Hajjar,A.M., Peterson,S.B., Borenstein,E. and Mougous,J.D. (2019) Human gut bacteria contain acquired interbacterial defense systems. *Nature*, **575**, 224–228.
3. Singh,K., Milstein,J.N. and Navarre,W.W. (2016) Xenogeneic silencing and its impact on bacterial genomes. *Annu. Rev. Microbiol.*, **70**, 199–213.
4. Lamberte,L.E., Baniulyte,G., Singh,S.S., Stringer,A.M., Bonocora,R.P., Stracy,M., Kapanidis,A.N., Wade,J.T. and Grainger,D.C. (2017) Horizontally acquired AT-rich genes in *Escherichia coli* cause toxicity by sequestering RNA polymerase. *Nat. Microbiol.*, **2**, 16249.
5. Dillon,S.C. and Dorman,C.J. (2010) Bacterial nucleoid-associated proteins, nucleoid structure and gene expression. *Nat. Rev. Microbiol.*, **8**, 185–195.
6. Flores-Ríos,R., Quatrini,R. and Loyola,A. (2019) Endogenous and foreign nucleoid-associated proteins of bacteria: occurrence, interactions and effects on mobile genetic elements and host's biology. *Comput. Struct. Biotechnol. J.*, **17**, 746–756.
7. Ishihama,A. and Shimada,T. (2021) Hierarchy of transcription factor network in *Escherichia coli* K-12: H-NS-mediated silencing and anti-silencing by global regulators. *FEMS. Microbiol. Rev.*, **45**, fuab032.
8. Navarre,W.W., Porwollik,S., Wang,Y., McClelland,M., Rosen,H., Libby,S.J. and Fang,F.C. (2006) Selective silencing of foreign DNA with low GC content by the H-NS protein in *Salmonella*. *Science*, **313**, 236–238.
9. Gordon,B.R., Li,Y., Cote,A., Weirauch,M.T., Ding,P., Hughe,T.R., Navarre,W.W., Xia,B. and Liu,J. (2011) Structural basis for recognition of AT-rich DNA by unrelated xenogeneic silencing proteins. *Proc. Natl. Acad. Sci. USA*, **108**, 10690–10695.

10. Japaridze,A., Yang,W., Dekker,C., Nasser,W. and Muskhelishvili,G. (2021) DNA sequence-directed cooperation between nucleoid-associated proteins. *iScience.*, **24**, 102408.
11. Dorman,C.J. and Ní Bhriain,N. (2020) CRISPR-Cas, DNA supercoiling and nucleoid-associated proteins. *Trends Microbiol.*, **28**, 19–27.
12. Bdira,F.B., Erkelens,A.M., Qin,L., Volkov,A.N., Lippa,A.M., Bowring,N., Boyle,A.L., Ubbink,M., Dove,S.L. and Dame,R.T. (2021) Novel anti-repression mechanism of H-NS proteins by a phage protein. *Nucleic Acids Res.*, **49**, 10770–10784.
13. Son,B., Patterson-West,J., Arroyo-Mendoza,M., Ramachandran,R., Iben,J.R., Zhu,J., Rao,V., Dimitriadis,E.K. and Hinton,D.M. (2021) A phage-encoded nucleoid associated protein compacts both host and phage DNA and derepresses H-NS silencing. *Nucleic Acids Res.*, **49**, 9229–9245.
14. Leung,K.Y., Wang,Q.Y., Yang,Z. and Siame,B.A. (2019) *Edwardsiella piscicida*: a versatile emerging pathogen of fish. *Virulence.*, **10**, 555–567.
15. Shao,S., Lai,Q.L., Liu,Q., Wu,H.Z., Xiao,J.F., Shao,Z.Z., Wang,Q.Y. and Zhang,Y.X. (2015) Phylogenomics characterization of a highly virulent *Edwardsiella* strain ET080813^{T} encoding two distinct T3SS and three T6SS gene clusters: propose a novel species as *Edwardsiella anguillarum* sp. nov. *Syst. Appl. Microbiol.*, **38**, 36–47.
16. Wang,Q.Y., Yang,M.J., Xiao,J.F., Wu,H.Z., Wang,X., Lv,Y.Z., Xu,L.Z., Zheng,H.J., Wang,S.Y., Zhao,G.P. *et al.* (2009) Genome sequence of the versatile fish pathogen *Edwardsiella tarda* provides insights into its adaptation to broad host ranges and intracellular niches. *PLoS One*, **4**, e7646.
17. Yang,M.J., Lv,Y.Z., Xiao,J.F., Wu,H.Z., Zheng,H.J., Liu,Q., Zhang,Y.X. and Wang,Q.Y. (2012) *Edwardsiella* comparative phylogenomics reveal the new intra/inter-species taxonomic relationships, virulence evolution and niche adaptation mechanisms. *PLoS One*, **7**, e36987.
18. Chen,H., Yang,D.H., Han,F.J., Tan,J.C., Zhang,L.Z., Xiao,J.F., Zhang,Y.X. and Liu,Q. (2017) The bacterial T6SS effector EvpP prevents NLRP3 inflammasome activation by inhibiting the Ca^{2+}-dependent MAPK-Jnk pathway. *Cell Host Microbe*, **21**, 47–58.
19. Yang,G.H., Billings,G., Hubbard,T.P., Park,J.S., Leung,K.Y., Liu,Q., Davis,B.M., Zhang,Y.X., Wang,Q.Y. and Waldor,M.K. (2017) Time-resolved transposon insertion sequencing reveals genome-wide fitness dynamics during infection. *mBio.*, **8**, e01581-17.
20. Yang,D.H., Liu,X.H., Xu,W.T., Gu,Z.Y., Yang,C.T., Zhang,L.Z., Tan,J.C., Zheng,X., Wang,Z., Quan,S. *et al.* (2019) The *Edwardsiella piscicida* thioredoxin-like protein inhibits ASK1-MAPKs signaling cascades to promote pathogenesis during infection. *PLoS Pathog.*, **15**, e1007917.
21. Rao,P.S., Yamada,Y., Tan,Y.P. and Leung,K.Y. (2004) Use of proteomics to identify novel virulence determinants that are required for *Edwardsiella tarda* pathogenesis. *Mol. Microbiol.*, **53**, 573–586.
22. Chakraborty,S., Sivaraman,J., Leung,K.Y. and Mok,Y.K. (2011) Two-component PhoB-PhoR regulatory system and ferric uptake regulator sense phosphate and iron to control virulence genes in type III and VI secretion systems of *Edwardsiella tarda*. *J. Biol. Chem.*, **286**, 39417–39430.
23. Liu,Y., Zhao,L.Y., Yang,M.J., Yin,K.Y., Zhou,X.H., Leung,K.Y., Liu,Q., Zhang,Y.X. and Wang,Q.Y. (2017) Transcriptomic dissection of the horizontally acquired response regulator EsrB reveals its global regulatory roles in the physiological adaptation and activation of T3SS and the cognate effector repertoire in *Edwardsiella piscicida* during infection toward turbot. *Virulence*, **8**, 1355–1377.
24. Chakraborty,S., Li,M., Chatterjee,C., Sivaraman,J., Leung,K.Y. and Mok,Y.K. (2010) Temperature and Mg^{2+} sensing by a novel PhoP-PhoQ two-component system for regulation of virulence in *Edwardsiella tarda*. *J. Biol. Chem.*, **285**, 38876–38888.
25. Yin,K.Y., Guan,Y.P., Ma,R.Q., Wei,L.F., Liu,B., Liu,X.H., Zhou,X.H., Ma,Y., Zhang,Y.X., Waldor,M.K. *et al.* (2018) Critical role for a promoter discriminator in RpoS control of virulence in *Edwardsiella piscicida*. *PLoS Pathog.*, **14**, e1007272.
26. Wei,L.F., Qiao,H.X., Sit,B., Yin,K.Y., Yang,G.H., Ma,R.Q., Ma,J.B., Yang,C., Yao,J., Ma,Y. *et al.* (2019) A bacterial pathogen senses host mannose to coordinate virulence. *iScience.*, **20**, 310–323.
27. Zhang,J., Xiao,J.F., Zhang,Y., Cui,S.L., Liu,Q., Wang,Q.Y., Wu,H.Z. and Zhang,Y.X. (2014) A new target for the old regulator: H-NS suppress T6SS secretory protein EvpP, the major virulence factor in the fish pathogen *Edwardsiella tarda*. *Lett. Appl. Microbiol.*, **59**, 557–564.
28. Cui,S.L., Xiao,J.F., Wang,Q.Y. and Zhang,Y.X. (2016) H-NS binding to *evpB* and *evpC* and repressing T6SS expression in fish pathogen *Ewardsiella piscicida*. *Arch. Microbiol.*, **198**, 653–661.
29. Gao,Z.P., Nie,P., Lu,J.F., Liu,L.Y., Xiao,T.Y., Liu,W., Liu,J.S. and Xie,H.X. (2015) Type III secretion system translocon component EseB forms filaments on and mediates autoaggregation of and biofilm formation by *Edwardsiella tarda*. *Appl. Environ. Microbiol.*, **81**, 6078–6087.
30. Gao,X.T., Wang,X.T., Mao,Q.Q., Xu,R.J., Zhou,X.H., Ma,Y., Liu,Q., Zhang,Y.X. and Wang,Q.Y. (2018) VqsA, a novel LysR-type transcriptional regulator, coordinates quorum sensing (QS) and is controlled by QS to regulate virulence in the pathogen *Vbrio alginolyticus*. *Appl. Environ. Microbiol.*, **84**, e00444-18.
31. Tjaden,B. (2015) *De novo* assembly of bacterial transcriptomes from RNA-seq data. *Genome Biol.*, **16**, 1.
32. Feng,J., Liu,T., Qin,B., Zhang,Y. and Liu,X.S. (2012) Identifying ChIP-seq enrichment using MACS. *Nat. Protoc.*, **7**, 1728–1740.
33. Xie,C., Mao,X.Z., Huang,J.J., Ding,Y., Wu,J.M., Dong,S., Kong,L., Gao,G., Li,C.Y. and Wei,L.P. (2011) KOBAS 2.0: a web server for annotation and identification of enriched pathways and diseases. *Nucleic Acids Res.*, **39**, W316–W322.
34. Basu,D., Khare,G., Singh,S., Tyagi,A., Khosla,S. and Mande,S.C. (2009) A novel nucleoid-associated protein of *Mycobacterium tuberculosis* is a sequence homolog of GroEL. *Nucleic Acids Res.*, **37**, 4944–4954.
35. Liu,Y., Wang,H.Y., Cui,T., Zhou,X.L., Jia,Y.X., Zhang,H. and He,Z.G. (2016) NapM, a new nucleoid-associated protein, broadly regulates gene expression and affects mycobacterial resistance to anti-tuberculosis drugs. *Mol. Microbiol.*, **101**, 167–181.
36. Minor,W., Cymborowski,M., Otwinowski,Z. and Chruszcz,M. (2006) HKL-3000: the integration of data reduction and structure solution–from diffraction images to an initial model in minutes. *Acta Crystallogr. D Biol. Crystallogr.*, **62**, 859–866.
37. Giacovazzo,C. and Siliqi,D. (2004) Phasing via SAD/MAD data: the method of the joint probability distribution functions. *Acta Crystallogr. D Biol. Crystallogr.*, **60**, 73–82.
38. Terwilliger,T.C., Adams,P.D., Read,R.J., McCoy,A.J., Moriarty,N.W., Grosse-Kunstleve,R.W., Afonine,P.V., Zwart,P.H. and Hung,L.W. (2009) Decision-making in structure solution using bayesian estimates of map quality: the PHENIX autosol wizard. *Acta Crystallogr. D Biol. Crystallogr.*, **65**, 582–601.
39. Adams,P.D., Grosse-Kunstleve,R.W., Hung,L.W., Ioerger,T.R., McCoy,A.J., Moriarty,N.W., Read,R.J., Sacchettini,J.C., Sauter,N.K. and Terwilliger,T.C. (2002) PHENIX: building new software for automated crystallographic structure determination. *Acta Crystallogr. D Biol. Crystallogr.*, **58**, 1948–1954.
40. Murshudov,G.N., Skubak,P., Lebedev,A.A., Pannu,N.S., Steiner,R.A., Nicholls,R.A., Winn,M.D., Long,F. and Vagin,A.A. (2011) REFMAC5 for the refinement of macromolecular crystal structures. *Acta Crystallogr. D Biol. Crystallogr.*, **67**, 355–367.
41. Potterton,E., Briggs,P., Turkenburg,M. and Dodson,E. (2003) A graphical user interface to the CCP4 program suite. *Acta Crystallogr. D Biol. Crystallogr.*, **59**, 1131–1137.
42. Emsley,P. and Cowtan,K. (2004) Coot: model-building tools for molecular graphics. *Acta Crystallogr. D Biol. Crystallogr.*, **60**, 2126–2132.
43. Afonine,P.V., Grosse-Kunstleve,R.W., Echols,N., Headd,J.J., Moriarty,N.W., Mustyakimov,M., Terwilliger,T.C., Urzhumtsev,A., Zwart,P.H. and Adams,P.D. (2012) Towards automated crystallographic structure refinement with phenix.refine. *Acta Crystallogr. D Biol. Crystallogr.*, **68**, 352–367.
44. Choi,J. and Groisman,E.A. (2020) Horizontally acquired regulatory gene activates ancestral regulatory system to promote *Salmonella* virulence. *Nucleic Acids Res.*, **48**, 10832–10847.
45. Desai,S.K., Winardhi,R.S., Periasamy,S., Dykas,M.M., Jie,Y. and Kenney,L.J. (2016) The horizontally-acquired response regulator SsrB drives a *Salmonella* lifestyle switch by relieving biofilm silencing. *eLife*, **5**, e10747.
46. Schiltz,C.J., Lee,A., Partlow,E.A., Hosford,C.J. and Chappie,J.S. (2019) Structural characterization of class 2 OLD family nucleases supports a two-metal catalysis mechanism for cleavage. *Nucleic Acids Res.*, **47**, 9448–9463.

47. Han,Y., Wei,L.F., Xiao,J.F., Zhang,Y.X., Wang,Q.Y. and Zhou,M. (2020) Identification and study of InV as an inverse autotransporter family representative in *Edwardsiella piscicida*. *Arch. Microbiol.*, **202**, 1107–1116.
48. Duan,B., Ding,P., Navarre,W.W., Liu,J. and Xia,B. (2021) Xenogeneic silencing and bacterial genome evolution: mechanisms for DNA recognition imply multifaceted roles of xenogeneic silencers. *Mol. Biol. Evol.*, **38**, 4135–4148.
49. Beamer,L.J. and Pabo,C.O. (1992) Refined 1.8 a crystal structure of the lambda repressor-operator complex. *J. Mol. Biol.*, **227**, 177–196.
50. Riccardi,E., van Mastbergen,E.C., Navarre,W.W. and Vreede,J. (2019) Predicting the mechanism and rate of H-NS binding to AT-rich DNA. *PLoS Comput. Biol.*, **15**, e1006845.
51. Stella,S., Cascio,D. and Johnson,R.C. (2010) The shape of the DNA minor groove directs binding by the DNA-bending protein Fis. *Genes Dev.*, **24**, 814–826.
52. Pérez-Morales,D., Banda,M.M., Chau,N.Y.E., Salgado,H., Martínez-Flores,I., Ibarra,J.A., Ilyas,B., Coombes,B.K. and Bustamante,V.H. (2017) The transcriptional regulator SsrB is involved in a molecular switch controlling virulence lifestyles of *Salmonella*. *PLoS Pathog.*, **13**, e1006497.
53. Will,W.R., Bale,D.H., Reid,P.J., Libby,S.J. and Fang,F.C. (2014) Evolutionary expansion of a regulatory network by counter-silencing. *Nat. Commun.*, **5**, 5270.
54. Groisman,E.A., Duprey,A. and Choi,J. (2021) How the PhoP/PhoQ system controls virulence and Mg^{2+} homeostasis: lessons in signal transduction, pathogenesis, physiology, and evolution. *Microbiol. Mol. Biol. Rev.*, **85**, e0017620.
55. Dillon,S.C., Espinosa,E., Hokamp,K., Ussery,D.W., Casadesús,J. and Dorman,C.J. (2012) LeuO is a global regulator of gene expression in *Salmonella enterica* serovar Typhimurium. *Mol. Microbiol.*, **85**, 1072–1089.
56. Newman,S.L., Will,W.R., Libby,S.J. and Fang,F.C. (2018) The curli regulator CsgD mediates stationary phase counter-silencing of *csgBA* in *Salmonella* Typhimurium. *Mol. Microbiol.*, **108**, 101–114.
57. Banda,M.M., Zavala-Alvarado,C., Pérez-Morales,D. and Bustamante,V.H. (2019) SlyA and HilD counteract H-NS-mediated repression on the *ssrAB* virulence operon of *Salmonella enterica* serovar Typhimurium and thus promote its activation by OmpR. *J. Bacteriol.*, **201**, e00530-18.
58. Cameron,A.D. and Dorman,C.J. (2012) A fundamental regulatory mechanism operating through OmpR and DNA topology controls expression of *Salmonella* pathogenicity islands SPI-1 and SPI-2. *PLos Genet.*, **8**, e1002615.
59. Pozdeev,G., Mogre,A. and Dorman,C.J. (2021) Consequences of producing DNA gyrase from a synthetic *gyrBA* operon in *Salmonella enterica* serovar Typhimurium. *Mol. Microbiol.*, **115**; 1410–1429.
60. Will,W.R., Navarre,W.W. and Fang,F.C. (2015) Integrated circuits: how transcriptional silencing and counter-silencing facilitate bacterial evolution. *Curr. Opin. Microbiol.*, **23**, 8–13.
61. Kane,K.A. and Dorman,C.J. (2011) Rational design of an artificial genetic switch: Co-option of the H-NS-repressed *proU* operon by the VirB virulence master regulator. *J. Bacteriol.*, **193**, 5950–5960.
62. Williamson,H.S. and Free,A. (2005) A truncated H-NS-like protein from enteropathogenic *Escherichia coli* acts as an H-NS antagonist. *Mol. Microbiol.*, **55**, 808–827.
63. Levine,J.A., Hansen,A.M., Michalski,J.M., Hazen,T.H., Rasko,D.A. and Kaper,J.B. (2014) H-NST induces LEE expression and the formation of attaching and effacing lesions in enterohemorrhagic *Escherichia coli*. *PLoS One*, **9**, e86618.
64. Winardhi,R.S., Gulvady,R., Mellies,J.L. and Yan,J. (2014) Locus of enterocyte effacement-encoded regulator (Ler) of pathogenic *Escherichia coli* competes off histone-like nucleoid-structuring protein (H-NS) through noncooperative DNA binding. *J. Biol. Chem.*, **289**, 13739–13750.
65. Ayala,J.C., Wang,H., Benitez,J.A. and Silva,A.J. (2018) Molecular basis for the differential expression of the global regulator VieA in *Vibrio cholerae* biotypes directed by H-NS, LeuO and quorum sensing. *Mol. Microbiol.*, **107**, 330–343.
66. García,J., Cordeiro,T.N., Prieto,M.J. and Pons,M. (2012) Oligomerization and DNA binding of Ler, a master regulator of pathogenicity of enterohemorrhagic and enteropathogenic *Escherichia coli*. *Nucleic Acids Res.*, **40**, 10254–10262.
67. Dame,R.T., Rashid,F.M. and Grainger,D.C. (2020) Chromosome organization in bacteria: mechanistic insights into genome structure and function. *Nat. Rev. Genet.*, **21**, 227–242.
68. Jiao,J., Zhang,B., Li,M.L., Zhang,Z. and Tian,C.F. (2022) The zinc-finger bearing xenogeneic silencer MucR in α-proteobacteria balances adaptation and regulatory integrity. *ISME J.*, **16**, 738–749.
69. Qin,L., Erkelens,A.M., Ben,Bdira.F. and Dame,R.T. (2019) The architects of bacterial DNA bridges: a structurally and functionally conserved family of proteins. *Open Biol*, **9**, 190223.